Check for updates

Water-induced erosion potentiality and vulnerability assessment in Kangsabati river basin, eastern India

Rabin Chakrabortty[1] · Subodh Chandra Pal[1] · Alireza Arabameri[2] ·
Phuong Thao Thi Ngo[3] · Indrajit Chowdhuri[1] · Paramita Roy[1] · Sadhan Malik[1] ·
Biswajit Das[1]

Abstract

The large-scale water-induced erosion is one of the most determining elements on land degradation in subtropical monsoon-dominated region. From this large-scale erosion, the fertility of the agricultural land has been decline consequently. So, estimation of the amount of erosion and its accurate prediction is necessary for escaping from this hazardous situation. In this study, the application of evidential belief function (EBF), spatial logistic regression (SLR) and ensemble of EBF and SLR to estimate the erosion potentiality with the help of ArcGIS and Soil and water assessment tool (SWAT). The average annual soil erosion has been estimated with the help of revised universal soil loss equation (RUSLE) and geographical information system (GIS). Apart from this to evaluate the importance of morphotectonic parameters on soil erosion, the correlation between erosion potentiality and average annual soil erosion has been quantified. In large-scale erosion, there is a direct impact of storm rainfall event in monsoon period in the entire subtropical region. Here, in erosion potentiality assessment, the optimal capacity of ensemble EBF-SLR is higher than the single alone methods, i.e., EBF and SLR. So, the mentioned approaches can be applied in soil erosion research in subtropical environment with considering the erosion causal parameters. This type of information can be helpful to the decision-maker and stakeholders to take proper initiative to reducing the rate of erosion. The main task of the future researcher is to implement this method more accurate ways with considering more reliable variables and slight modifications of the approaches in keeping in the view of regional environment.

Keywords Average annual soil erosion · Land degradation · Morphotectonic parameters · Soil erosion · Soil and water assessment tool

✉ Subodh Chandra Pal
geo.subodh@gmail.com

Extended author information available on the last page of the article

1 Introduction

The nature and as well as human-induced activity plays a important role to fluctuate the availability of natural resource (land, water, mineral etc.) in wide volume (Gajbhiye et al., 2014). Surface soil erosion establishes land degradation in severe form which is responsible for decline crop production (Pal & Chakrabortty, 2019a; Saha et al., 2021). This type of surface erosion is very common in process and massively accelerated by the artificial activities. In this process, the amount of total loss is much more than the formation of regolith (Lal, 2003, 2014; Nearing, 2013; Renard et al., 2011; Wischmeier & Smith, 1978). This problem is posed by the tropical and subtropical areas in an extreme stage by reducing the resource capacity. Management is really very realistic at the level of the watershed, defining many variables in relation to the hydro-geomorphological characteristics. Different researchers from multiple domains find out the risk for watershed degradation by prioritizing the watercourse with specific factors in mind (Aher et al., 2014; Saha et al., 2020). Comparably, several researchers determined the quantity of erosion by taking into account various quantitative and semiempirical methods for evaluating vulnerable areas (Gelagay & Minale, 2016; Kouli et al., 2009; Lin et al., 2002).

Geospatial tools (Remote sensing and Geographical information system) are more powerful method for evaluating morphometric characteristics in the watercourses to evaluate the probability for erosion (Avinash et al., 2011; Chowdary et al., 2009; Meshram & Sharma, 2017; Rahmati et al., 2016; Yadav et al., 2014). Several academics used SWAT (Soil and water conservation tool) and the GIS for calculating the various morphometric variables with appropriate precision (Fadil et al., 2011). The SWAT is a mixture of multiple statistical and computation methods, capable of accurately estimating the complicated procedure. It separates the catchment from compact to separate drainage, HRU and reach then; the sub-watershed could be demarcated by statistical measure.

In water-induced processes, various morphometric variables have a different purpose to erode the surface materials. Recently, the 56 percent out of total land deteriorated due to rapid rate of erosion (Oldeman, 1992). One of the important reasons for land loss is the conversion of the vegetative area into farming and impervious areas (Alejandro & Omasa, 2007). This case, in United Nation, stated that is an obstacle to sustainable development because it cannot support ecological and forestry policy without adequate calculation assessment of degradation and being integrated into strategic planning (Thomas et al., 1991).

The implementation of artificial intelligence (AI) approaches in the geographic information system has frequently applied in recent times to estimate the rate of catchment erosion (Korb & Nicholson, 2010). In addition, these AI techniques permitted in use of network analysis to integrate the qualitative information (Arabameri et al., 2021; Martınez et al., 2003; Pal et al., 2020). This model conducts in nonlinear feature and partners each neuron linked to a consequent neighbor and it is functionality varying to improve the network for effective results. This related the hidden layer feature makes a variation between input and output result being acted as a defining factor for a nonlinear connection (Chowdhuri et al., 2020; Koskivaara, 2004). The unevenness of rainfall from low to heavy is a major reasons that show the possibility of future erosion area, its volume and deposition (Pal & Chakrabortty, 2019a). The erratic rainfall, wet season, a short period of torrential rainfall occurrence with high intensities, etc., of the whole region is controlled by monsoon. Consequently, the possible effect of rainfall fluctuations is isolated from the important characteristics of estimating erosion rate upcoming time frame (Teng et al., 2018).

Besides, the LULC (Land use and land cover) changes on variance of rainfall have been calculated with high accuracy. This current research has tried to predict how land erosion has evolved over the years through various activities (Natural and artificial). Scientific and lasting research effect on the development of surface land features can be obtained in this way. Commitment of land cover and change of vegetation field related to constructional environment and its surrounding environment: anthropogenic behavior transforms land use pattern and environment do play role also. Land cover is one of the main significant data is used to illustrate the impacts of changes in land use. A map of land use is generated using various techniques on satellite data. Many research on Landsat's satellite data created land use maps of the monitored classification method. The improvements in urban planning and sustainable areas across time were measured by the use of land cover maps. The adjustment in land cover through time and shifting of people from core to periphery area is normally influenced by climatic variation (temperature, wind, rain and drought) that individuals feel insecure in the region because the development and scheduling are not good. A few researches show the spectrum of bioclimatic console areas that people are comfortable with. Changes of the soil and the climatic conditions are quite significant. Soil evaluations offer citizens in town an aggressive scenario to prevent the negative economic and political issues. New research including spatial data can predict the drought conditions and management strategies (Cetin & Sevik, 2016a ; Cetin, 2015a, b, c; Kaya et al., 2019). Temperature, wind, rain, drought influence climatic variables that peoples are feel confident or unconfident in the area because of the bad strategy and maintenance capacity. A few of the studies show the spectrum of comfortable bioclimatic comfort zone where people feel quite relax mood. Dryness assessment is very important, as in the climatic scales. Dry environment assessments provide residents with an active urban environment and ensure that the economic and political challenges are detrimental. Latest analysis using remotely sensed drought conditions data indicates drought management (Cetin, 2015c; Cetin & Sevik, 2016a, b; Cetin et al., 2018a, b; , 2019; Kaya et al., 2019). The new analysis is to create a conservation plan focused on the objectives of preserving a region's ecological and historic landscape principles by evaluating landscape parameters same as the list of possible tourists, vegetation cover, cultural norms, and elevation composition. ArcGIS has been used as a geographic information system to test the terrain parameters, and the data from the analysis were collected through a questionnaire, surveys and visualization. The region has a wildly heterogeneous topographical structure, i.e., it has a rich surface-shaped structure and hence has visible landscape importance. The diversity in surface features also allows the region to enrich in green cover and with climatic values; Apart from that locational benefit can be called this diversity. This allowed rich flora and thus wide range of fauna to be formed. The characteristics of summer and winter season are hot and cool in nature, respectively, in this region and also derives adequate rainfall in winter (Cetin, 2015a, b, c; Cetin & Sevik, 2016a, b; Cetin et al., 2018a, b, 2019).

Morphotectonic variables have a major effect on the vulnerability to soil erosion in India, a monsoon-dominated subtropical region. Hence, these variables not only lead an important role in the hydro-geomorphic properties, also by integrating the factors to estimate the vulnerability to soil erosion. Geophysical characteristics and their behavior are known to control soil erosion due to the fact that the entire catchment area is concerned with absorbing the exterior water and eroding topmost layers and eventually transported them by the various active drivers. The river and its drainage network play a significant part in the development of the environment (Patel et al., 2013). The measurement by morphotectonic variables of the characteristics of the diverse environment is important for the possibility for erosion (Clarke, 1966; Kottagoda & Abeysingha, 2017). Measurement of such variables will make a scientific

real scenario about the changes in relief and land that can be differentiated from one to the other (Strahler, 1964). Diverse morphometric variables, groundwater potential (Avinash et al., 2011), erosion possibility and others have been extensively for this reason.

The application of various experimental models is very reliable in watershed scale for estimating the rate of erosion with optimal accuracy. The various kinds of models have been used by various researches in diversified discipline, such as USLE (Universal soil loss equation), RUSLE (Revised universal soil loss equation), MMF (Morgan–Morgan–Finney method), RMMF (Revised Morgan–Morgan–Finney method), Chinese soil erosion model, and European soil erosion model. Of them, the RUSLE (Revised universal soil loss equation) is more reliable in monsoon-dominated region, where the impact of rainfall event is prominent. This model is very flexible in nature and can be used in various climatic regions with little modification. The main objectives of this outcome are to estimate the erosion potentiality using ensemble EBF and spatial logistic regression and quantify the average annual soil erosion by RUSLE model. And find out the relationship between amount of erosion in the entire region and erosion potentiality in sub-watershed scale.

1.1 Literature reviews

Our soil resource is critical to humanity's survival. It not only provides the absolute basis for our lives, but it also provides the majority of farming products that support us and our mode of living, fiber, and timber. Soil loss is a worldwide issue that is now one of the most pressing concerns in many countries. Soil erosion refers to the loss of soil caused by natural (e.g., water, wind, and snow) and human-induced (e.g., vigorous and widespread agricultural production) forces working together (Nasir Ahmad et al., 2020). Since soil quality damage is almost always irreversible, ensuring agricultural production and environmental quality requires preserving this resource (Chen, 2007). Wind and water erosion are two of the most common risks to soil health. This is a natural mechanisms that affects our lives in a variety of ways, the most serious of which is decreased food supply (Oliver & Gregory, 2015; Pimentel, 2006). Erosion causes off-site sediment transport, which may create complications downstream in contrast to on-site soil depletion (Enters, 1998). Sediment can clog irrigation systems, raise the risk of floods, reduce reservoir capacity, and transport nutrients and pollutants, both of which undermine water quality (Mostaghimi et al., 2000). As a result, reducing erosion is critical not just for protecting soil but also for maintaining potable water supply and enhancing water and air quality. Engineers and others have made significant strides in understanding and controlling erosion in recent decades. Increased demographic stresses on land use and crop productivity, on the other hand, continue to cause new and enhanced soil erosion challenges (Blaikie & Brookfield, 2015). We previously described the recent trends of research regarding the erosion potentiality and average annual soil loss with considering different empirical and semiempirical methods. Apart from this, a detailed comprehensive literatures has been incorporated for understanding the recent trends of research in related to soil erosion and the justification of our research (Table 1).

2 Case study

The 'River Kangsabati' initiate from the Chhota Nagpur plateau's Jabourban hill in Puruliya district, which is regarded to be major undulating degradation-prone gully terrain (Fig. 1) where the primary stream of first and second order is involved

Table 1 A comprehensive literatures in different parts of the world

Location	Considerable methods	Key findings	References
Iran	Various machine learning algorithms, namely boosted regression trees (BRT), deep learning (DL), and multiple linear regression (MLR)	From this research, it has been established that the BRT is most optimal model than any other model used in this analysis	Sahour et al., (2021)
Iran	Spatiotemporal monitoring of soil erosion using G2 model	The findings, which include mean annual, seasonal, and quarterly soil erosion for each of the country's 7 main basins and 30 sub-basins, are applicable to lawmakers. The findings can be used to improve planting patterns and the position of biological soil management activities such that ground cover productivity is maximized during the most erosive era	Mohammadi et al., (2021)
China	Effects of the undecomposed layer and semi-decomposed layer on soil erosion	The results of this analysis contribute to a better understanding of how litter controls slope erosion and serve as a guide for effectively managing soil erosion	Liu et al., (2021)
Turkey	Temporal and spatial soil erosion with considering revised universal soil loss equation (RUSLE) and conditional probability	The bulk of soil characteristics are dynamic and change over time as a result of changing climatological patterns, other external exposures, and land management practices. If the degree of confusion about each datum increases, soil data loses its consistency across time	Baskan, (2021)
China	Revised universal soil loss equation (RUSLE) with improves support practice (C) factor	In this analysis, the RUSLE with enhanced P factor taking different SWC measures performed well, as evidenced by soil erosion measurement information from specific runoff plots with slope gradients of 15–35°	Tian et al., (2021)
India	Revised universal soil loss equation (RUSLE) with different ensemble GCM model	Soil erosion is expected to increase in the future (2040, 2060, 2080, and 2100 years). So, in sub-topical monsoon-dominated nations like India, the possible effect of climate change on soil loss has been developed. In a densely populated landscape like India, caused by human activity activity-induced land cover change is the primary cause of climate change and extreme soil depletion, which has a direct effect on land fertility, growth, and, as a result, socioeconomic impact	Pal et al., (2021)

Table 1 (continued)

Location	Considerable methods	Key findings	References
India	Analytical neural network (ANN), geographically weighted regression (GWR) and ensemble of GWR–ANN	For assessing water-induced soil erosion vulnerability, the ensemble GWR–ANN outperforms the GWR, ANN. Since soil erosion is not a one-way mechanism, the multifaceted effects of predictor variables must be calibrated correctly by taking into account all potential factors and choosing the best models for particular environment	Chakrabortty et al., (2020b)

in diminishing the soil (Mittal et al., 2014). This circumstance, the importance role of first and second order channels helps make this basin into the central portion is very sloping and rocky terrain. This river flows primarily southeast into the lower Bengal basin to its mouth (Mittal et al., 2014), and it is regarded to become major water scare region, though it experiences adequate precipitation during the peak monsoon period (Chakrabortty et al., 2020a). The larger amount of rainfall with maximum kinetic forces produces severe situation for flooding and also soil loss and related sedimentation. This region is bounded by the northeast basin of the Damodar River, and the southeast basin of the Subarnarekha River. Diversified geographical, hydrological and environmental attributes are typical distinctiveness of such a river basin that can stimulate the greater attention of economic resources. The Kangsabati dam is situated at the Kangsabati confluence location, which is one of the Kumari River's main tributaries. This is a multi-purpose program that can promote irrigation, potable water, fish farming, and hospitality. It reduces the effect of drought in their area of command. In recent years, however, due to extreme erosion and subsequent sedimentation, storage capacity has been declining in 1/3 in its yearly capacity (Bhave et al., 2014).

3 Methods

This research is associated with estimating the erosion potentiality with considering evidential belief function (EBF), spatial logistic regression (SLR) and ensemble of EBF and SLR (Fig. 2). Apart from this, the average annual soil loss also estimated with the help of
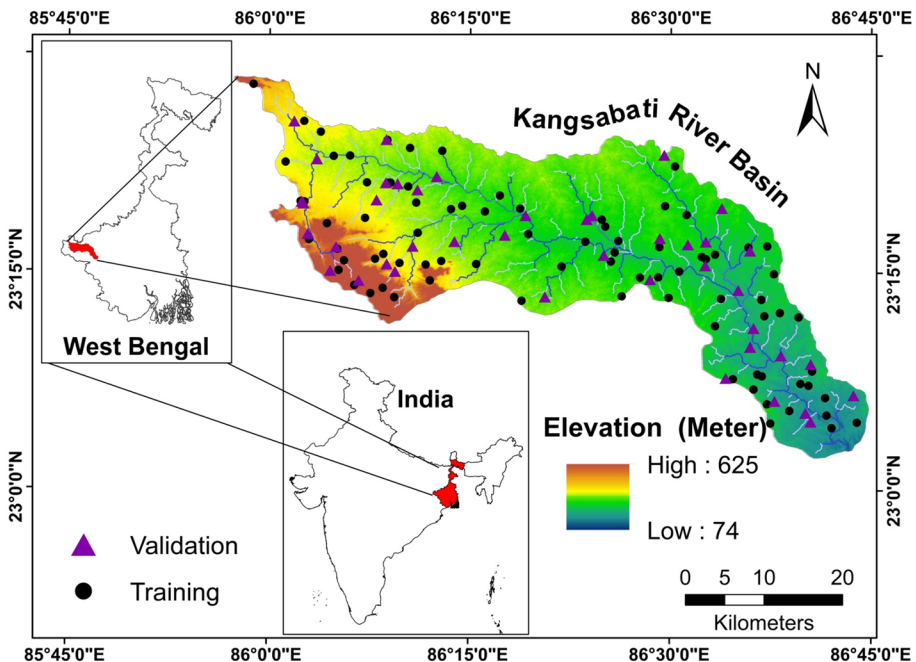

Fig. 1 Location of the study area

revised universal soil loss equation (RUSLE). The detailed method for estimating the soil loss with considering RUSLE is shown in Fig. 3. The correlation between erosion potentiality and average annual soil loss has been done to find out the relationship among the role of morphotectonic factors on soil erosion.

3.1 Data sources

Different datasets have been chosen, such as topographical chart, DEM (Digital elevation model) derived from SRTM (Shuttle radar topographic mission), geological chart, and line map. Besides this, different primary knowledge about the erosional dimension is required for this work to be carried out. The source of the data is indicated in Table 2.

3.2 Watershed delineation through soil and water assessment tool (SWAT)

SWAT in GIS platform was regarded to delineate the Kangsabati River Basin watershed. The SWAT model is important for determining the HRUs (Hydrologic response units) to recognize watersheds and sub-watersheds (Mittal et al., 2014). The distinctive variation of relief and geo-hydrological interaction is expressed of each component. The SWAT model has been considered to determine and classify various sub-basin factors, model of rainfall and runoff (Bauwe et al., 2016), model of infiltration, estimation of erosion and related catchment-wise sedimentation, simulation of nutrition etc. In SWAT, HRUs are one of the essential methods employed extensively in various fields. The Soil and Water
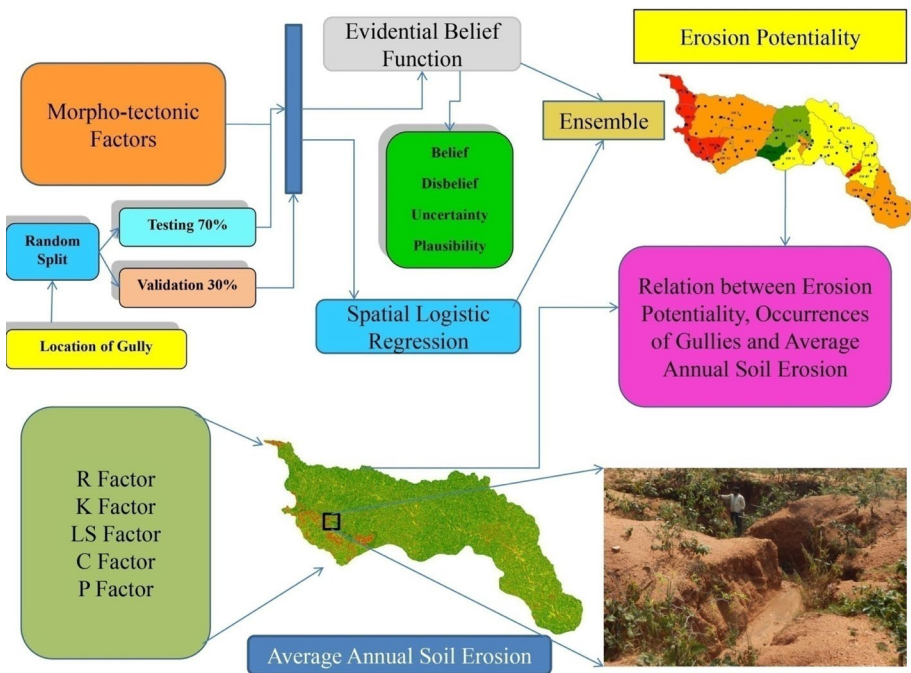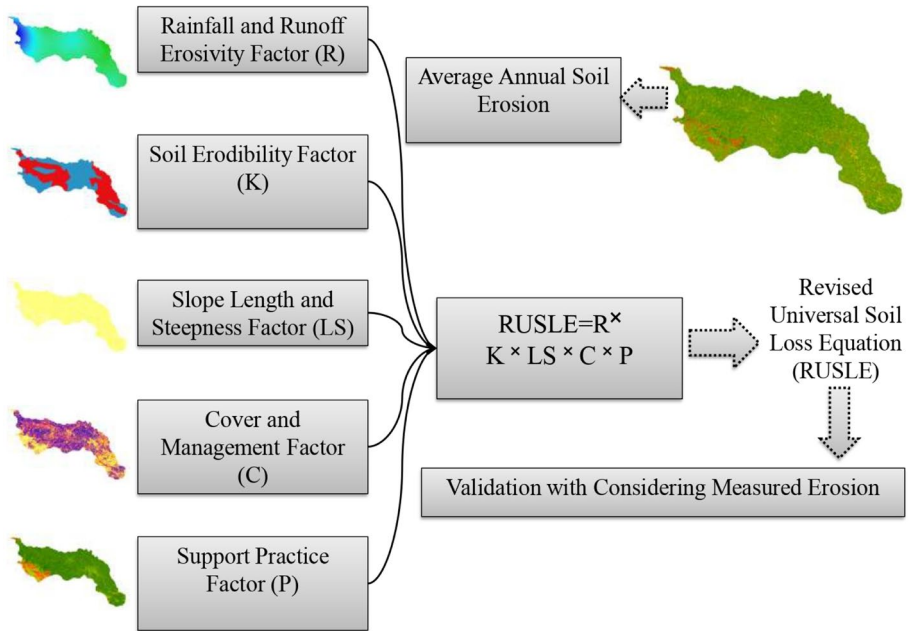

Fig. 2 Methodology Flow Chart

Fig. 3 Detail method for estimating the average annual soil erosion

assessment Tool (SWAT) has been considered for extracting 19 sub-watersheds and estimation of its associated morphometric parameters.

3.3 Selection of the causative factors

Utilizing evidential belief function, the mentioned probabilistic variables for erosion were chosen to evaluate the ability for erosion. The causes of causality are static as well as dynamic. Table 3 shows the rationale behind preference of this static and dynamic component.

3.4 Approaches for estimating erosion potentiality

In this research, the erosion potentiality in watershed scale has been estimated with the help of evidential belief function (EBF), spatial logistic regression (SLR) and ensemble of EBF and SLR. The ensemble approach is more optimistic regarding the perdition of different environmental hards that already established by different researchers (Arabameri et al., 2020; Band et al., 2020a, 2020b), so we considered this ensemble approach for estimation of erosion potentiality.

Table 2 Database and its sources

Parameters	Data type	Data source	Data details
Slope length and steepness factor	Raster grid	ALOS PALSAR DEM, (Alaska Satellite Facility)	12.5 m spatial resolution
Geology (detailed lithology and deposits)	Line, point and polygon coverage	Geological Survey of India	1:63,300
NDVI	Spatial/raster grid	Sentinel 2A (European Space Agency)	10 m spatial resolution
LULC	Spatial/raster grid	Sentinel 2A (European Space Agency)	10 m spatial resolution
Soil texture	Soil sample	Primary observation and laboratory analysis	Same resolution with other parameters
Soil moisture index	Soil sample	Primary observation and laboratory analysis	Same resolution with other parameters
Soil erodibility	Soil sample	Primary observation and laboratory analysis	Same resolution with other parameters
Rainfall and runoff erosivity factor	Station specific information	Primary observation	Interpolation with same resolution in respect to other parameters
Elevation	Raster Grid	ALOS PALSAR DEM, (Alaska Satellite Facility)	12.5 m spatial resolution
Slope gradient (degree)	Raster grid	ALOS PALSAR DEM, (Alaska Satellite Facility)	12.5 m spatial resolution

Table 3 Evidences for selection of morphotectonic parameters

Morphotectonic factors	Reason for selection
Basin Relief	It is highly positive in the creation and growth of drainage, the sum of runoff, land mass absorption and surface layer erosion
Ruggedness number	It is among the essential measures of capacity for erosion and seems to be effective of estimating surface disturbance (Strahler, 1957). The landscape 's structural heterogeneity is also reflected by the roughness number (Schumm, 1956)
Mean slope	The quantity and orientation of the gradient can be managed by the complex geomorphological behavior (Ghosh & Guchhait, 2016). These mechanisms of the top soil erosion are closely associated to the design of the slope gradient
Dissection index	It typically shows the risk of structural erosion and shows the levels of landscape growth and transformation (B. and Thornbury 2006; Avinash et al., 2011; Pareta & Pareta, 2011)
Average relief	It affects drainage properties and their related energy to erode the surface structures. Those higher values may imply the significant potential for erosion, and vice versa
Drainage density	The Quality of runoff and wetness conditions is quite important with respect to the extent of the drainage rate. The internal and external effect of drainage density is expressed in various physiographical properties in association with geomorphic influences, landscape growth, connection of natural vegetation (Kelson & Wells, 1989; Moglen et al., 1998; Oguchi, 1997). The quantity of drainage density is highly positive for the capacity for erosion in response to stormy rainfall events (Richard, 1968)
Mean bifurcation ratio	Geophysical conditions and their regulation of drainage features are obtained by means of the bifurcation ratio (Strahler, 1957). It can quantify the capacity for erosion of the river basin as well as the dissection
Stream number	From it, the density and existence of the drainage could be established. The number of the stream has an important function in terms of runoff volume and strength
Drainage texture ratio	The climatic patterns, LULC, rock form, soil properties, and landscape stage of growth are derived from it. This feature can change the intensity of surface penetration and a strong connection among texture and density is formed (Ozdemir & Bird, 2009)
Infiltration number	The number of infiltration includes the level of infiltration and overflows (Strahler, 1964) there has been a differentiated correlation between the quantity of penetration and the volume of runoff
Length of overland flow	It is correlated with the catchment areas complex geophysical characteristics. It is close to sheet flow to some degree and there is a significant effect of rainfall and its relevant soil runoff properties (Kanth & Hassan, 2012)
Elongation ratio	A significant influencing component that can affect the quantity of runoff is the elongation ratio. The basin's evolutionary step can be prepared in the form it
Circularity ratio	The dendritic process of the watershed area is indicated, and that potentiality of erosion is indicated
Form factor	It is a measure to distinguish various basin shapes (Horton, 1932) and is responsible of representative the flow strength, so this factor directly and indirectly affects the erosion risk
Geology	Geomorphic features are very important in terms of morphometric properties and possibilities for erosion (Chakrabortty et al., 2020a). Varied geophysical connection is more likely to be susceptible to erosion, as concerns per field of research

Table 3 (continued)

Morphotectonic factors	Reason for selection
Lineament density	Lineaments govern the surface water flow, and also the sub-surface flow pattern and instances. The river canals are regulated by lineaments location and direction. That significantly influences the potential for erosion. Since the analysis is located with the structural hills and pediments, this form of aspect is therefore very important in terms of erosion

3.4.1 Estimation of the erosion potentiality using EBF

EBF relies on the 'Dempster–Shafer principle' concept originally introduced by the Dempster (Dempster, 1968), which is derived from the 'Bayesian probability theory' (Tehrany et al., 2017). The key benefit of this approach is the versatility of implementing different functions from several origins. Dempster – Shafer methodology is concerned with showing that the theory is correct with fact, so this approach is one of the important predictor considered by GIS (Malpica et al., 2007) in the multiple fields. There have been four evidential belief features which are connected in this task, those were belief component, disbelief component, uncertainty component and plausibility component (Feizizadeh et al., 2014). Belief and plausibility are the lower and greater forced of the likelihood. In a defined series, uncertainty is essentially the difference among feature of belief and feature of plausibility. Incredulity is the feature that is focused on the conviction of being incorrect (Tehrany et al., 2017).

$$\text{Belcf}_{ij} = \frac{\text{Wcf}_{ij}D}{\sum_{i=1}^{n} \text{Wcf}_{ij}D} \tag{1}$$

$$\text{Wcf}_{ij}D = \frac{\left[N\left(C_{ij} \cap D\right)/N(D)\right]}{\left[\left\{N\left(C_{ij}\right) - N\left(C_{ij} \cap D\right)\right\}/\left\{N(T) - N(D)\right\}\right]} \tag{2}$$

$$\text{Discf}_{ij} = \frac{\text{Wcf}_{ij}\bar{D}}{\sum_{i=1}^{n} \text{Wcf}_{ij}\bar{D}} \tag{3}$$

$$\text{Wcf}_{ij}\bar{D} = \frac{\left[\left\{N(D) - N\left(C_{ij} \cap D\right)\right\}/N(D)\right]}{\left[N(T) - N(D) - N\left(C_{ij}\right) + N\left(C_{ij} \cap D\right)\right]/[N(T) - N(D)]} \tag{4}$$

$$\text{Unccf}_{ij} = 1 - \text{Belcf}_{ij} - \text{Discf}_{ij} \tag{5}$$

$$\text{Plscf}_{ij} = \text{Belcf}_{ij} + \text{Unccf}_{ij} \text{ Or } \text{Plscf}_{ij} = 1 - \text{Discf}_{ij} \tag{6}$$

where $Belcf_{ij}$ is the conviction value of jth class of the ith soil loss favorable parameters, $\text{Wcf}_{ij}D$ is the importance of cf_{ij} that wires the belief that eroding process is further dominant than the cohesiveness of landform or conception of regolith, $N\left(C_{ij} \cap D\right)$ is the number of g, $N(D)$ is the gully points, $N\left(C_{ij}\right)$ is the particular region, $N(T)$ is the total part, $Discf_{ij}$ is the incredulity significance of the ith soil erosion causal factors, $\text{Wcf}_{ij}\bar{D}$ is the weight of cf_{ij} which emphasis the environments resistance was most current than soil loss, $Unccf_{ij}$ is

the confusion significance of the jth-class related parameters for erosion and $Plscf_{ij}$ is the plausibility attribute of the jth erosion causative variables class ith.

$$\mathrm{Bel}_{f_{1f_2}} = \frac{\mathrm{Bel}_{f_1}\,\mathrm{Bel}_{f_2} + \mathrm{Bel}_{f_1}\,\mathrm{Unc}_{f_2} + \mathrm{Bel}_{f_2}\,\mathrm{Unc}_{f_1}}{\beta} \tag{7}$$

$$\mathrm{Dis}_{f_{1f_2}} = \frac{\mathrm{Dis}_{f_1}\,\mathrm{Dis}_{f_2} + \mathrm{Dis}_{f_1}\,\mathrm{Unc}_{f_2} + \mathrm{Dis}_{f_2}\,\mathrm{Unc}_{f_1}}{\beta} \tag{8}$$

$$\mathrm{Unc}_{f_{1f_2}} = \frac{\mathrm{Unc}_{f_1}\,\mathrm{Unc}_{f_2}}{\beta} \tag{9}$$

$$\mathrm{Pls}_{f_{1f_2}} = \mathrm{Bel}_{f_{1f_2}} + \mathrm{Unc}_{f_{1f_2}} \tag{10}$$

where Bel is the certainty component for every issues or variety, Dis is the disbelief component for every issues or variety, Unc is the level of improbability for every issues or variety and $\beta = 1 - \mathrm{Bel}_{f_1}\,Dis_{f_2} - \mathrm{Dis}_{f_1}\,\mathrm{Bel}_{f_2}$ is a regularizing feature which satisfies that, Bel + Unc + Dis = 1. EBFs of maps f3... f_n are mutual relationship of all function concurrently in a organized technique by using Eqs.10–13.

3.4.2 Application of spatial logistic regression for erosion potentiality

Logistic regression is a categorical determining variable that relates to several self-determining variables. The regression variables predict the existence and absence of dependent variables (Yilmaz, 2009). The logistic regression algorithm used to convert dependent variables to log variables that apply maximum probability estimates. The benefit of SLR is that all types of independent variables were used for logistic regression algorithms meaning that variables can be regular or categorical (Lee, 2007). For multivariate models, the SLR coefficient was used to determine the ratio of each independent variable to the dependent variables (Pradhan, 2010). The factors and the dependent variable are numerical and the dependent variables for the SLR algorithm must have nominal data. Many studies have been using the forward, backward stepwise and enter logistic regression method but enter method gets all regression coefficients. Now all regression coefficients are required for further raster calculation, and the spatial logistic regression has produced a flood susceptibility maps. Statistically, the SLR algorithm is represented as below Eq. 11 and 12 with the association of independent (morphotectonics parameters) and dependent (gully points) variables. (Gorsevski et al., 2006; Lee, 2007; Pradhan, 2010).

$$P = \frac{1}{(1 + e^{-z})} \tag{11}$$

$$Z = b_0 + b_1 x_{1+} b_2 x_2 + \ldots + b_n x_n \tag{12}$$

In Eq. 11, P is the forecasted erosion potentiality, the potentiality value on the S-shaped curve ranges from 0 to 1 and z is the linear amalgamation and state in the subsequent equation. Eq. 12, b_0 is the model's constant, the bi (i = 1, 2, …, n) is the SLR model's slope or coefficients and the xi (i = 1, 2, …, n) are the self-determining parameters. Binary LR is the non-spatial model, and the data are spatially auto-correlated. Therefore, by modifying

any expression, the spatial structure is part of the logistic regression function. Now the modified equation below can help with spatial logistic regression (SLR). Three items are important in this spatial autocorrelation: spatial weight matrix (W), spatial autocorrelation parameter (p) and error term that obeys a Gaussian distribution (ε). The spatial erosion potentiality measured through below Eq. 13–16 (Erener & Düzgün, 2012; Yang et al., 2019).

$$W = \begin{bmatrix} 0 & f(d_{12}) & \cdots & f(d_{ij}) \\ f(d_{21}) & 0 & \ldots & f(d_{2j}) \\ \vdots & \vdots & \ddots & \vdots \\ f(d_{i1}) & f(d_{i2}) & \ldots & 0 \end{bmatrix} \tag{13}$$

$$f(d_{ij}) = \frac{d_{ij}}{\sum_1^j d_{ij}} \tag{14}$$

$$L = y \ln \frac{\exp(a + X\beta + \rho Wy)}{1 + \exp(a + X\beta + \rho Wy)} - (1 - y)\ln(1 + \exp(a + X\beta + \rho Wy)) \tag{15}$$

$$Z = b_0 + b_1 x_{1+} b_2 x_2 + \ldots + b_n x_n + \rho WY + \varepsilon \tag{16}$$

ρWY is the spatial arrangement consequence motivated by spatial correlation. Where W is the weight matrix and $f(d_{ij})$ is the inverse weighting functions which expressed as Eq. 19. ε Is the concept of error flouting a Gaussian function. L is the integrated nested Laplacian approximation to reduced time during calculation (Yang et al., 2019).

3.4.3 Estimation of erosion potentiality using ensemble EBF-SLR

Here, EBF and SLR are integrated with GIS framework to take the strengths of both representation and describe with adequate precision the area of favorable for erosion. The below approaches for measuring the potentiality of erosion in GIS platform are regarded:

$$\begin{aligned} EP_{EBF\text{-}SLR} = &\; \text{Basin Relief}\left(\frac{EBF + SLR}{2}\right) + \text{Ruggedness Number}\left(\frac{EBF + SLR}{2}\right) + \text{Mean Slope}\left(\frac{EBF + SLR}{2}\right) \\ &+ \text{Dissection Index}\left(\frac{EBF + SLR}{2}\right) + \text{Average Relief}\left(\frac{EBF + SLR}{2}\right) \\ &+ \text{Drainage Density}\left(\frac{EBF + SLR}{2}\right) + \text{Mean Bifurcation Ratio}\left(\frac{EBF + SLR}{2}\right) \\ &+ \text{Stream Number}\left(\frac{EBF + SLR}{2}\right) + \text{Drainage Texture Ratio}\left(\frac{EBF + SLR}{2}\right) \\ &+ \text{Infiltration Number}\left(\frac{EBF + SLR}{2}\right) + \text{LengthoftheOverland}\left(\frac{EBF + SLR}{2}\right) \\ &+ \text{ElongationRatio}\left(\frac{EBF + SLR}{2}\right) + \text{CirculatoryRatio}\left(\frac{EBF + SLR}{2}\right) \\ &+ \text{Form Factor}\left(\frac{EBF + SLR}{2}\right) + \text{Geology}\left(\frac{EBF + SLR}{2}\right) + \text{Lineament Density}\left(\frac{EBF + SLR}{2}\right) \end{aligned} \tag{17}$$

where EP is the capacity for erosion, EBF is the role of belief and SLR is the spatial logistic regression.

3.4.4 Application of RUSLE for estimation of soil erosion

A different factor has been considered for quantifying average annual soil loss with the help of revised universal soil loss equation (RUSLE).

The rainfall and runoff erosivity factor (R) factor of this region has been estimated with considering the storm rainfall even in monsoon period (Fig. 4a). This is the most significant aspect in soil erosion modeling in subtropical areas. This factor was predictable with the aid of subsequent equation:

$$R = \sum_{i=0}^{12} 1.735 \times 10^{\left(1.5 \log_{10} \left(\frac{P_i^2}{P} \right) - 0.08188 \right)} \tag{18}$$

where R is the R factor and it expresses in MJ/ha/year.

We have estimated the different physical and chemical parameters from the collected samples for preparing the soil erodibility factor (with considering the pH, organic matter, textural properties and bulk density), soil moisture index etc. (Fig. 4b). For soil
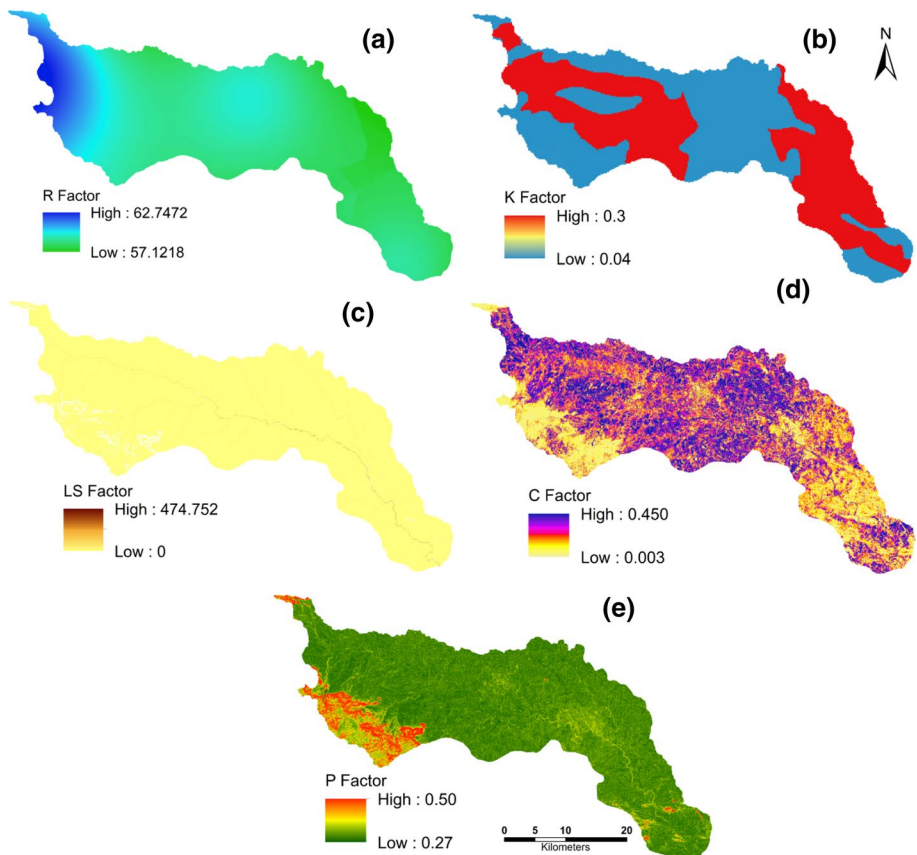

Fig. 4 Parameters of RUSLE model; R factor (a), K factor (b), LS Factor (c), C Factor (d) and P factor (e)

erodibility (K) factor, following method is considered with allowing the different elemental properties of the soil:

$$K = 0.0137 \times \left(0.2 + 0.3 \times e^{\left[-0.0256 \times \text{San} \times \left(\frac{1-\text{Sil}}{100} \right) \right]} \right) \times \left(\frac{\text{Sil}}{\text{Cla} + \text{Sil}} \right)^{0.3}$$
$$\times \left[1 - \frac{0.25 \times \text{TOC}}{\text{TOC} + e^{(3.72 - 2.95 \times TOC)}} \right] \times \left[1 - \frac{0.7 \times \text{SN}_1}{\text{SN}_1 + e^{(22.9 \times SN_1 - 5.51)}} \right] \tag{19}$$

where San is the proportion of sand, Sil is the proportion of silt, Cla is the proportion of clay and SN_1 is the 1-San/100 (Teng et al., 2018).

The slope length and steepness (LS) factor has been estimated from the DEM with considering following equation (Fig. 4c):

$$\text{LS} = (m + 1) \times \left[\frac{A_s}{22.} \right] \times \left[\frac{\sin\beta}{0.0896} \right] \tag{20}$$

$$A_s = \frac{1}{b_1} \sum_{i=1}^{N} a_1 u_1 \tag{21}$$

where As is the slope extent in meter and β is the position of slope (Chakrabortty et al., 2020b).

For estimating the cover and management (C) factor, the NDVI and its threshold have been considered. The quantity of vegetation cover with seasonal variation is one of the most determining elements of soil erosion model. So, this information is very important in subtropical region regarding the status of erosion in catchment scale (Fig. 4d).

$$\text{NDVI} = \frac{(\text{NIR} - \text{Red})}{(\text{NIR} + \text{Red})} \tag{22}$$

Then, the exponential function of NDVI algorithm is considered for determining the C factor raster in GIS platform (Malik et al., 2019; Pal et al., 2018):

$$C = \exp \left[-a \frac{\text{NDVI}}{(\beta - \text{NDVI})} \right] \tag{23}$$

where a and β are the unit fewer parameters, which is capable of estimating the curve between NDVI and its associated C factor. This scenario gives better prediction in an exponential way in comparison with the linear association (Pal & Shit, 2017). The support practice (P) factor usually shows the quantity of soil erosion from a region with specific practices of protection (Fig. 4e). P factor simulates the influence of support approaches which reduce the average annual soil loss rate. It represents the percentage of soil loss connected with a distinct situation from similar mitigation support activities to equal loss in up- and down-slope farming practices.

For estimating the average annual soil erosion, the factors (R, K, LS, C and P) of RUSLE have been integrated in GIS platform. The following method has been considered for creating the soil erosion raster with considering the pixel information of each factor (Pal & Chakrabortty, 2019b):

$$A = R \times K \times \text{LS} \times C \times P \tag{24}$$

4 Results and discussion

4.1 Assessment of morphotectonic variables and its impact on soil loss

Different morphometric parameters have been quantified with the established empirical equation in GIS environment. Table 4 represents the process for measuring descriptions of all morphometric elements. Here, established approaches and GIS platform have been considered for estimating the morphometric parameters in this region.

4.1.1 Landscape parameter

BR (basin relief) is measured using variations within a watershed among maximum and altitude. It is liable for watershed geophysical features (Sreedevi et al., 2009). The BR difference will act as an important function in the various watersheds of erosive operations.

Table 4 Methods for estimating the causality factors

Morphometric attributes	Equation
Watershed area (Wa)	Calculated in GIS platform
Watershed perimeter (Wp)	Calculated in GIS platform
Basin length (Lb)	Length of the maximum length
Stream order (μ)	Hierarchical order
No. of streams (Nμ)	Watershed-wise total number of all streams
Length of stream (Lu)	Linear element of channel
Mean length of streams (Lsm)	$L_{\mathrm{sm}} = \frac{L_u}{N_\mu}$
Frequency of stream (Fs)	$F_s = \frac{N_\mu}{w_a}$
Drainage density (Dd)	$D_{\mathrm{d}} = \frac{L_u}{w_a}$
Bifurcation ratio (Rb)	$R_b = \frac{N_\mu}{N_\mu + 1}$
Mean bifurcation ratio (Rbm)	standard assessment of bifurcation ratio
Drainage texture ratio (Rt)	$R_t = \frac{N_\mu}{w_p}$
Infiltration number (If)	$I_f = F_s \times D_d$
Length of overland flow (Lof)	$L_{of} = \frac{1}{D_d} \times 2$
Ruggedness number (Rn)	$R_n = D_d \times \frac{B_r}{1000}$
Watershed relief (Br)	$B_r = H_{max} - H_{min}$
Dissection index (Di)	$D_i = \frac{B_r}{H_{max}}$
Maximum relief (Hmax)	Highest elevation
Minimum relief (Hmin)	Lowest elevation
Average relief (Ar)	$A_r = \frac{H_{\max} - H_{\min}}{2}$
Mean slope (Mslp)	In GIS platform
Form factor (Rf)	$R_{\mathrm{f}} = \frac{W_a}{L_{b^2}}$
Elongation ratio (Re)	$R_{\mathrm{e}} = \frac{2}{L_b} \times \frac{w_a}{0.5}$
Circularity ratio (Rc)	$R_{\mathrm{c}} = 4 \times \pi \times \frac{W_a}{W_p^2}$

BR ranges around 83 and 417 mt. SW 2 and SW3 display very high (363–417) BR (Fig. 5a). The strong (182–363) BR is in SW- 1, 4, 5 and 12. SW-13, 14, and 19 are considered to be the mild BR (118–182) The low BR is observed in SW 6, 8, 10, 11, 15 and 16. The very low BR (83–96) occurs in SW- 7, 9 and 18. Contrasted to other section of the river system the western section is occupied by the higher BR.

Ruggedness number (Rn) is the topography's elongated character and is vulnerable to flooding. The erosity is thus effectively linked to the high Rn. The very high Rn values (7.66–9.85) distributed primarily at SW 7 and SW 15. The high Rn values (5.45–7.66) are observed in SW- 6, 8, 9, 10, 11, 16, 17 and 18 (Fig. 5b). And, relative to many other catchments in this region, these watersheds are susceptible to erosion. The medium Rn values (2.58–5.45) are distributed at SW- 13, 14 and 19. The Rn values at low (2.07–2.58) are 1, 3, 5 and 12. The very weak intense Rn values are in SW 2 and 4. The mean slope (MS) was measured in individual watersheds using the SWAT model. All pictoral information was taken into account for the determination of the MS. The fluvial actions are directly and indirectly affected by the slope quantity and its alignment. The quantity and orientation of runoff are greatly affected by the curvature of the slope, which is favorable for the
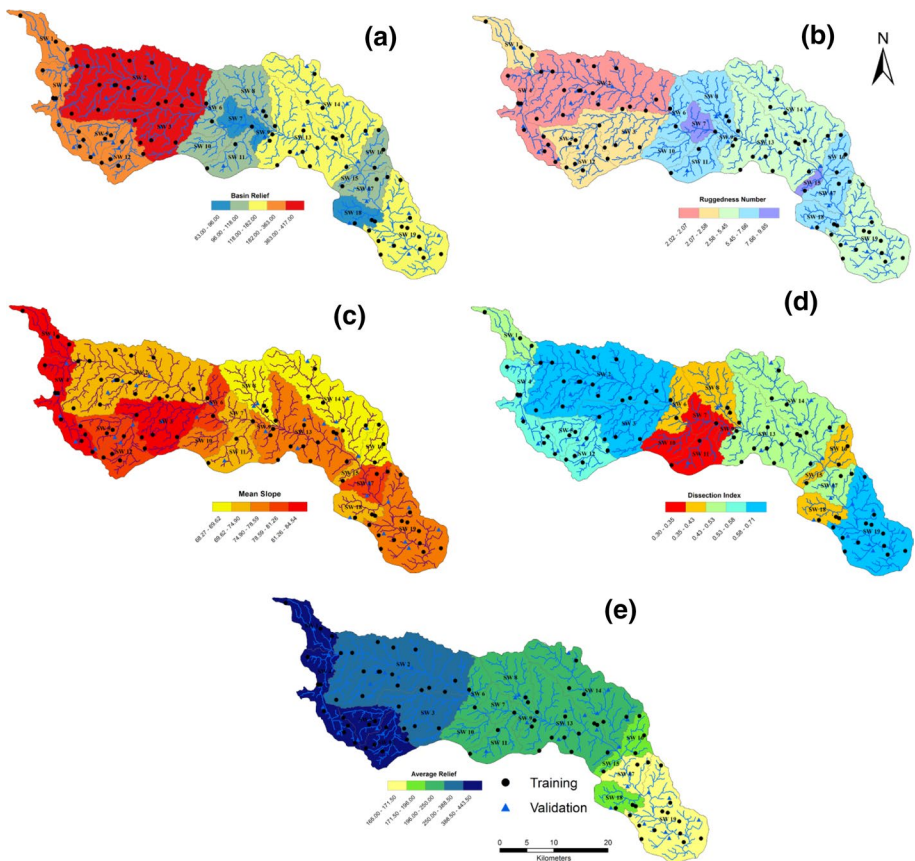

Fig. 5 Landscape Parameter: Basin Relief (a), Ruggedness Number (b), Mean Slope (c), Dissection Index (d), Average Relief (e)

loss of topsoil. The very high MS values (81.26–84.54) were found mainly in SW 1, 3, and 4 (Fig. 5c). The large MS values (78.59–81.26) occur in SW- 5,6,12 and 17. The medium MS values (47.90–78.50) are found at SW- 9, 10, 13, and 19. The MS values which are low (69.27–74.90) are 2, 7, 11, 15 and 18. The very low MS values (68.27–69.62) are centered in SW 8, 14 and 16. The DI (Dissection Index) of a specific river basin signifies the vertical eroding ability that made a significant contribution to the quantity of overflow and its related erosion (. DI values differ from 0 to 1; nearest to 0 suggests the exclusion of perpendicular cutting and nearest to 1 suggests the predominant vertical cutting feature correlated with this basin. The exceptionally high DI values (0.58–0.71) distributed primarily in SW 2, 3 and 19 (Fig. 5d). The high DI values (0.53–0.58) are found in SW- 4, 5, and 12. The medium DI values (0.43–0.53) are distributed at SW- 13, 14 and 17. The DI values at low (0.35–0.43) are 6, 8, 15, 16 and 18. The extremely low DI values (0.30–0.35) are distributed in SW 2, 3, and 19. Average relief (AR) affects the larger runoff that can raise the level of erosion within the catchment. The very high AR values (388.50–443.50) distributed mostly in SW 1, 4, 5 and 12 (Fig. 5e). The high AR values (250.00–388.50) are given in SW 2 and 3. The medium (196.00–250.00) AR values are centered in SW- 15, 16 and 18. The low AR values (171.50–196.00) are given in 6, 7, 8, 9, 10, 11, 13 and 14. The found very low AR values (165.00–171.50) are in SW 17 and 19. The typical river basin relief indicates rapid curve variability from the river source point to the mouth of the river.

4.1.2 Areal parameter

Drainage density (DD) is one of the prevailing features that overlap between their length and scope on the basis of the interaction of both orders. It is closely related to the basic geophysical series and its components, and the quantity of vegetation and other related relief elements are covered up. High DD shows greater surface runoff volumes and less stimulation capacity. It implicitly reduces groundwater recharge. The very high DD values (> 0.83) distributed mainly at SW 9 (Fig. 6a). The high DD values (0.76–0.83) are given in SW 1, 4, 11 and 18. The medium DD values (0.71–0.76) are distributed at SW- 14, 16, and 17. The low DD values (0.53–0.71) are found at 6, 7, 8, 10, 12 and 13. The distributed DD values in SW 2, 3 and 5 are very low (< 0.53).

Mean bifurcation ratio (Rb) is the relation among the total number of particular order streams and the whole amount of higher order streams (Horton, 1945). For the lowest possible overland flow, low Rb with fewer structural influences is favorable. But high Rb is very beneficial during the storm rainfall period for heavy flash flooding (Kanth & Hassan, 2012). The very high Rb values (4.14–7.34) centered mainly at SW 19. The high Rb values (2.69—4.14) are observed in SW 13 and 14 (Fig. 6b). The medium Rb values (1.44–2.69) are located in SW- 1, 2, 3, 12, 15, 16 and 18. The low Rb values (0.32–1.44) are found at 4, 5, 7, 8, 9 and 11. The concentrated Rb values in SW 6 are very small (< 0.32). The mean Rb of the entire river basin shows the overall river basin's high erosion capacity, since the bifurcation among the lowest order is very high. The maximum ratio among first and second order is generally positive about erosion tolerance. The number of a stream channel (SN) with its spatial distribution in a given order is recognized as stream number. The very high SN values (2.85–3.48) concentrated mainly at SW 5. The high SN values (1.54–2.85) are given in SW 15 and 17. The medium SN values (0.95–1.54) are distributed at SW- 2, 3, 8, 12, 13, 14 and 19. The low SN values (0.69–0.95) are given in 1, 4, 9 and 18 (Fig. 6c). The intense SN values in SW 6, 7, 10, 11 and 16 are very small (0.42–0.69). Watersheds erosion events are regulated by various geophysical and environmental
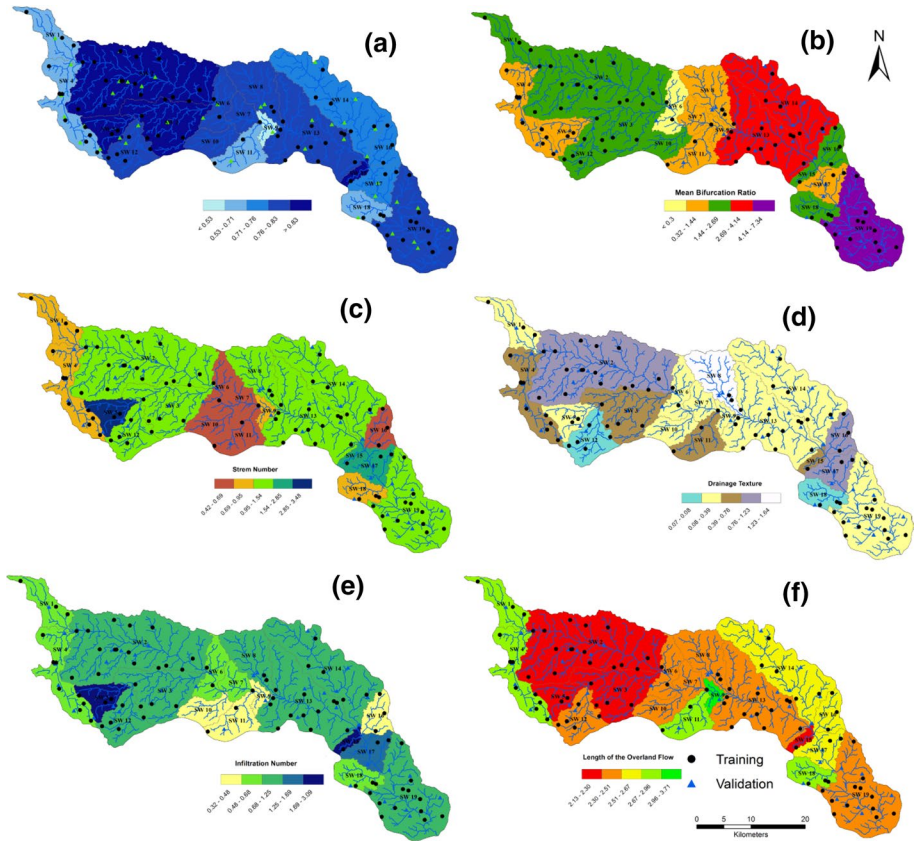
Fig. 6 Areal Parameter: Drainage Density (a), Mean Bifurcation Ratio (b), Stream Number (c), Drainage Texture Ratio (d), Infiltration Number (e), Length of the Overland Flow (f)

components, such as rainfall volume and quantity, soil hydrogeology, infiltration capability, soil humidity and soil formation process (Hembram & Saha, 2020). The DTR and its related causal factors typically control the susceptibility to the erosion. The very high DTR values (1.23–1.64) mostly centered in the SW 8. The high (0.76–1.23) DTR values are noticed in the SW 2, 16 and 17 (Fig. 6d). The medium DTR values (0.39–0.76) are found in SW- 3, 4, 11 and 15. The DTR values at low (0.08–0.39) are 1, 5, 6, 7, 9, 10, 13, 14 and 19. The concentrated very low DTR values (0.07–0.08) were in SW 12 and 18. Infiltration number (IN) shows the essence of the rock planes conductivity and the erosion nature of a particular region. The larger IN values usually confirm the surface penetrability and are not prone to erosion. Lower values are highly suitable with respect to probable for erosion. The very high IN values (1.69–3.09) are distributed mostly in the SW 5 and 15. The high IN values (1.25–1.69) appear in the SW 17. The medium IN values (0.68–1.25) are centered at SW- 2, 3, 8, 12, 13, 14 and 19 (Fig. 6e). The IN values which are small (0.48–0.68) are 1, 4, 6, 7 and 18. The exceptionally small IN values (0.32–0.48) distributed in SW 9, 10, 11 and 16. The amount of the quasi-channel water flow over the entire drainage area is called LOF. The flow transforms into a channel after that and circulates according to the initial

gradient. The removal of the top soil units from the upper layer is very important, and the conversion of these substances is also very positive. The very high LOF values (2.96–3.71) distributed mostly in the SW 9 (Fig. 6f). The high LOF values (2.67–2.96) are found on SW 1, 4, 11 and 18. The medium LOF values (2.51–2.67) are clustered at SW-14, 16, and 17. The low LOF values (2.30–2.51) are found in 6, 7, 8, 10, 13 and 19. The distributed LOF values in SW 2, 3, 5 and 15 were very small (2.13–2.30).

4.1.3 Shape parameter

The elongation ratio (ER) indicates, in particular, the developmental parts and their longitudinal river basin. With the involvement of neo-tectonics, it reveals the preceding stage of landscape development but also less elongated form means the exclusion of high runoff potential (Hembram & Saha, 2020). The very high ER values (0.23–0.36) distributed primarily in the SW 12, 16, 18 and 19. The high ER values (0.22–0.23) occur in SW 1, 2, 5, 10 and 11 (Fig. 7a). The medium ER values (0.20–0.22) are distributed at SW- 7, 8, and 17. The low ER values (0.15–0.20) are found to be 3, 13, 14 and 15. The distributed ER values in SW 4, 6, and 9 are very small (0.13–0.15). Here, SW 4, 6 and 9 are highly suitable for erosion and SW 12, 16, 18 and 19 are helpful for erosion conflict.

Circulatory ratio (CR) is openly linked to the amount and nature of the release and is affected by several components such as drainage, terrain, surface component, geological connection, and LULC (Miller, 1953). Higher CR shows the exterior ruggedness while minor values suggest low ruggedness. The very high CR values (0.59–0.74) mainly found in the SW 9. The high CR values (0.53–0.59) are given in SW 1, 4, 11 and 18 (Fig. 7b). The moderate CR values (0.50–0.53) are distributed at SW 14, 16, and 17. The low CR values (0.46–0.50) are: 6, 7, 8, 10, 12, 13 and 19. The very small CR values (0.43–0.46) clustered at SW 1, 3, 5 and 15.
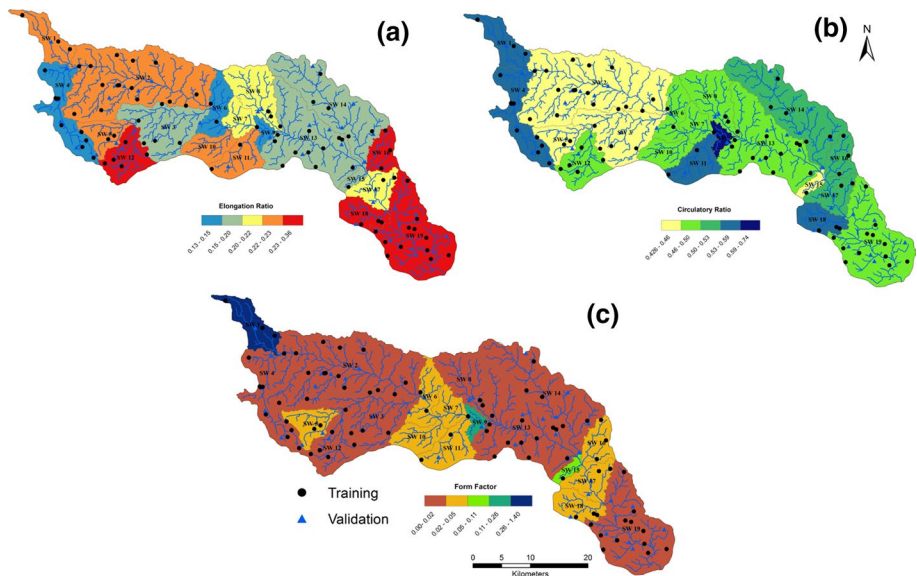

Fig. 7 Shape Parameter: Elongation Ratio (a), circulatory Ratio (b), Form Factor (c)

Table 5 Major geological unit and its ages

Sl No	Unit	Age
1	Fluvial sediments	Quaternary
2	Manbhum granite	Mesoproterozoic
3	Chhota Nagpur gneissic complex	Proterozoic (undifferentiated)
4	Unclassified metamorphics	Archaean—proterozoic
5	Dalma volcanics	Archaean—proterozoic
6	Singhbhum Gp	Palaeoproterozoic
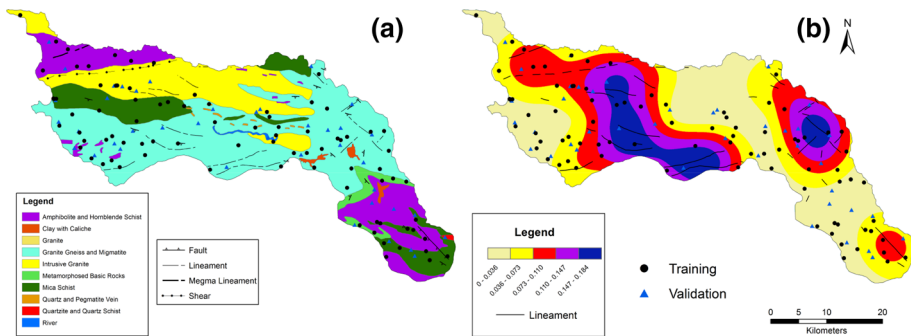
Fig. 8 Tectonic Parameter; Geology (a), Lineament Density (b)

Form Factor (FF) is one of the main aspects of the relationship between the watershed zone and the watershed span (Schumm, 1956). The higher FF value explains the circular form of the catchment whereas the lower value shows the elongated one (Rai et al., 2018). The very high FF values (0.26–1.40) mostly distributed in the SW 1. The SW 9 includes the strong (0.11–0.26) FF values. In SW 15 the medium FF values (0.05–0.11) are high. The low FF values (0.02–0.05) are given in SW 5, 6, 7, 10, 11, 16, 17 and 18 (Fig. 7c). The exceptionally low FF values (0.00–0.02) distributed in SW 2, 3, 4, 8, 12, 13, 14 and 19.

4.1.4 Tectonic parameter

This area is consistent with different forms of rock configuration that has an important position feature concerning the capacity for erosion (Table 5). The disruptive granite and associated rocks are dominating the upper division of this region. Intrusive granite and some associated rocks are dominating the middle portion of his region (Fig. 8a). Metamorphosis of simple rock with assemblage of some common element is dominating the lower part of this region. This river basin has witnessed various stratigraphic division that belonging to the tertiary-quaternary system of the oldest systems. In the most moment of each year, the whole regions of such a basin witnessed physical weathering in massive level. The western segment is the prolonged part of the Chota Nagpur that is the division of earliest Gondwana territory. The rate of regolith formation is directly related with the nature of bed rock and its associated climatic condition of the region. The degree of weathering is closely related with the nature of surface materials and availability of moisture.

Sufficient availability of water can accelerate the amount of chemical weathering and which is responsible for loss of the top soil. Weathering is a common mechanism in the process of landscape development and is responsible for landscape change.

Structural properties like unconformities can be represented in different ways on the earth's surface, including joints, cracks, bedding plains and foliations. Lineaments are commonly related to fracturing faults and linear regions, bent curvature and enhanced crust conductivity. Lineament has a strong effect on the possibility of erosion. The water movement is important for weakening the substances in the joint, cracks. Hydraulic gradient may play a critical function in the direction and association of lineaments. Besides this massive-scale erosion, the quantity and position of the lineaments are explicitly linked (Fig. 8b). Fault, lineament, megma lineament, and shear were considered for the estimation of lineament density. Not only lineaments, the traces of joints, anomalous forms of drainage, structural trends are also responsible for complex hydro-geomorphic characteristics of any region. The stability of the landscape is very much dependent on the nature of the structural elements. The very high (0.174–0.184) LD in the center part of the river basin is mainly extreme. The high LD (0.110–0.147) is located in the river basin's middle and northeast part. The moderate LD (0.073–0.110) is distributed in the river basin's western and northeastern portions. The low LD (0.036–0.073) is found in the river basin's western, northern, northeastern, and eastern part. The very low (0.000–0.036) LD was concentrated in the river basin's western, central, and eastern portions.

4.1.5 Estimation of erodibility by EBF model

A total of 16 influencing parameters were used to classify the probability for erosion. The possibility of potential for erosion is stand on the function of belief, unbelief, uncertainty and plausibility. The role of belief varies from 0.13 to 1.00 and some spatial variations occur in this region (Fig. 9). The values of the disbelief feature vary from 0.051 to 0.742 which is different from the function of the beliefs. Uncertainty and plausibility function values vary from 0.012 to 0.178 and 0.21 to 0.93, respectively.

4.2 Relation among erosion potentiality and erosion causal elements

The study reveals that the strong (182.00–363.00) BR has a stronger position in erosion potentiality than supplementary region relief levels. The small (96.00–118.00) BR amounts perform the reverse position with regard to erosion potentiality (Table 6). Very low (2.02–2.07) RN is favorable for potential erosion which supports the model's belief function. On the other hand, high RN (5.45–7.66) reveals the lower potential for erosion. Lower (68.27–69.62) MS promotes the beliefs feature in the potentiality for erosion but on the other hand high Ms is associated with lower probability for erosion. High (0.53–0.58) DI regions are advantageous or close proximity to erosion potential but very high (0.58–0.71) DI is not desirable for erosion potential. Another factor such as the DI is correlated with moderate feature on propensity for erosion. Very high (388.50–443.50) AR plays a significant role in erosion possibility but on the other side moderate AR (196.00–250.00) performs a different function in erosion potentiality. The AR is correlated with the modest feature in erosion possibility. Moderate DD (0.71–0.76) is connected with very low erosion potential but in this point of view, very low DD (<0.53) is related with different function. Very high erosion possibility is linked with very high (4.14–7.34) MBR regions which sustain the belief feature but very low MBR (0.10–0.32) plays the different role in
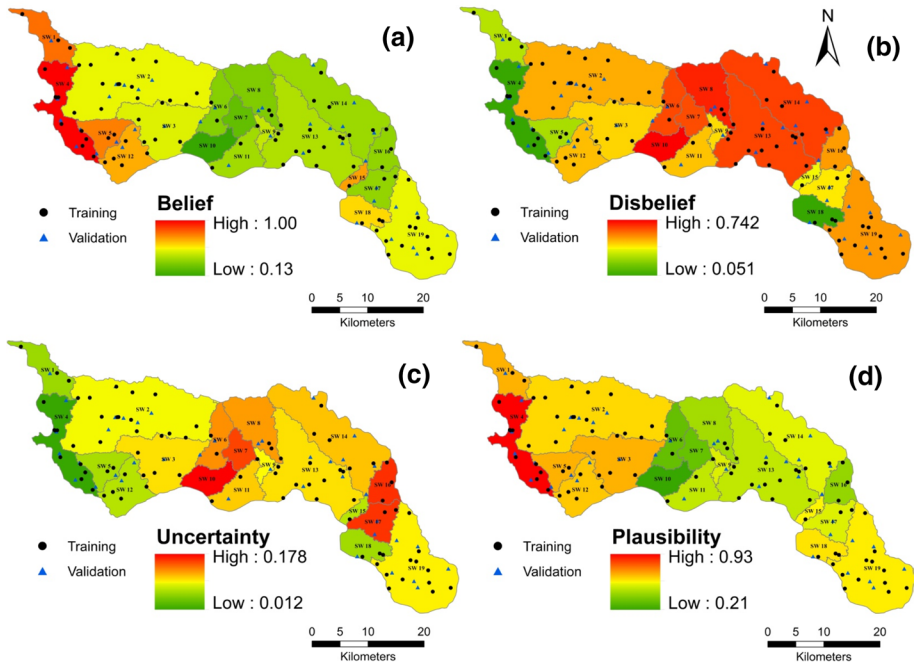
Fig. 9 Belief Function (**a**), Disbelief Function (**b**), Uncertainty Function (**c**) and Plausibility Function (**d**)

the propensity for erosion. The low SN (0.69–0.95) is highly optimistic about the capability for erosion but on the other hand very low SN values (0.42–0.69) are not optimal for the prospects for erosion. Low (0.39–0.76) DTR is highly prone to erosion but the very high (1.23–1.64) DTR is correlated with significantly different erosion prospective feature. Very high (1.69–3.09) IN is positive in erosion possibility which supports the belief component of EBF but very low (0.32–0.48) IN with less belief function plays the adverse impacts in erosion possibility. Very low OLF (2.13–2.30) is positive with respect to the capacity for erosion but higher OLF (2.30–2.51) is correlated with lower potential for erosion. The very low (0.13–0.15) ER is optimistic with respect to the potential for erosion but the moderate (0.20–0.22) ER is linked to lower erosion capacity. The high CR (0.53–0.59) is highly optimistic in terms of the possibilities for erosion but the moderate (0.50–0.53) CR areas have the adversely impacts in the potential for erosion. The moderate (0.05–0.11) SF values play the key role in the capacity for erosion but the strong (0.11–0.26) SF values are not positive with respect to the possibility for erosion. In the geological features, clay with caliche is positive in the possibility for erosion but Granite plays the reverse effect in the possibility for erosion. In nature, the role of other structures in the capacity for erosion is moderate. The low LD (0.036–0.073) is very much positive in respect to the erosion possibility but very high LD has a reverse effect in erosion possibility.

4.3 Prioritization of watershed on the basis of erosion potentiality

The sub-watershed-wise erosion capacity has find out considering various causality variables for erosion and their related breaking threshold in EBF model. The very high erosion

Table 6 Parameter-wise EBF and its sub-indices for erosion potentiality estimation

Sl. No	Parameter	Class	Area	No. of gully point	Belief	Disbelief	Uncertainty	Plausibility
1	Basin relief	83.00–96.00	76.383	4	0.162	0.201	0.637	0.799
		96.00–118.00	280.011	11	0.120	0.217	0.663	0.783
		118.00–182.00	485.053	31	0.200	0.189	0.611	0.811
		182.00–363.00	215.915	18	0.266	0.184	0.550	0.816
		363.00–417.00	374.357	19	0.157	0.209	0.634	0.791
2	Ruggedness number	2.02–2.07	347.107	28	0.342	0.173	0.485	0.827
		2.07–2.58	243.166	14	0.238	0.200	0.562	0.800
		2.58–5.45	485.053	25	0.212	0.212	0.576	0.788
		5.45–7.66	318.347	14	0.179	0.214	0.606	0.786
		7.66–9.85	38.047	2	0.216	0.200	0.584	0.800
3	Mean slope	68.27–69.62	261.753	10	0.212	0.216	0.572	0.784
		69.62–74.90	393.056	20	0.206	0.210	0.585	0.790
		74.90–78.59	375.458	24	0.188	0.192	0.619	0.808
		78.59–81.26	175.938	10	0.197	0.200	0.603	0.800
		81.26–84.54	225.514	19	0.179	0.182	0.640	0.818
4	Dissection index	0.30–0.35	124.430	3	0.073	0.218	0.709	0.782
		0.35–0.43	190.889	12	0.198	0.203	0.599	0.797
		0.43–0.53	263.325	21	0.256	0.187	0.557	0.813
		0.53–0.58	169.837	15	0.286	0.190	0.524	0.810
		0.58–0.71	535.122	32	0.188	0.202	0.611	0.798
5	Average relief	165.00–171.50	201.841	14	0.202	0.191	0.607	0.809
		171.50–196.00	80.068	7	0.260	0.191	0.549	0.809
		196.00–250.00	559.539	23	0.116	0.237	0.647	0.763
		250.00–388.50	374.357	19	0.145	0.207	0.648	0.793
		388.50–443.50	215.915	20	0.277	0.175	0.548	0.825

Table 6 (continued)

Sl. No	Parameter	Class	Area	No. of gully point	Belief	Disbelief	Uncertainty	Plausibility
6	Drainage density	<0.53	13.058	1	0.247	0.199	0.554	0.801
		0.53–0.71	206.166	17	0.267	0.185	0.548	0.815
		0.71–0.76	233.126	10	0.133	0.210	0.656	0.790
		0.76–0.83	557.112	32	0.181	0.201	0.618	0.799
		>0.83	422.258	23	0.171	0.205	0.624	0.795
7	Mean bifurcation ratio	0.10–0.32	41.118	2	0.165	0.199	0.636	0.801
		0.32–1.44	312.024	24	0.268	0.179	0.552	0.821
		1.44–2.69	593.525	28	0.159	0.226	0.614	0.774
		2.69–4.14	324.288	17	0.178	0.204	0.618	0.796
		4.14–7.34	160.765	12	0.260	0.191	0.550	0.809
8	Stream number	0.42–0.69	185.566	8	0.139	0.206	0.655	0.794
		0.69–0.95	171.364	15	0.296	0.184	0.520	0.816
		0.95–1.54	985.814	48	0.158	0.274	0.568	0.726
		1.54–2.85	51.932	3	0.189	0.198	0.612	0.802
		2.85–3.48	37.044	2	0.176	0.199	0.625	0.801
9	Drainage texture ratio	0.07–0.08	92.835	7	0.252	0.194	0.554	0.806
		0.08–0.39	685.863	35	0.166	0.222	0.612	0.778
		0.39–0.76	238.153	18	0.253	0.185	0.562	0.815
		0.76–1.23	345.166	20	0.190	0.198	0.612	0.802
		1.23–1.64	69.703	3	0.139	0.201	0.660	0.799

Table 6 (continued)

Sl. No	Parameter	Class	Area	No. of gully point	Belief	Disbelief	Uncertainty	Plausibility
10	Infiltration number	0.32–0.48	130.315	6	0.161	0.197	0.642	0.803
		0.48–0.68	351.245	17	0.170	0.203	0.627	0.797
		0.68–1.25	985.814	54	0.194	0.217	0.589	0.783
		1.25–1.69	41.076	2	0.171	0.193	0.636	0.807
		1.69–3.09	47.901	4	0.304	0.189	0.506	0.811
11	Length of overland flow	2.13–2.30	422.258	34	0.260	0.165	0.575	0.835
		2.30–2.51	557.112	23	0.128	0.238	0.634	0.762
		2.51–2.67	233.126	10	0.133	0.209	0.657	0.791
		2.67–2.96	206.166	15	0.233	0.190	0.577	0.810
		2.96–3.71	13.058	1	0.246	0.198	0.556	0.802
12	Elongation ratio	0.13–0.15	130.269	12	0.309	0.187	0.504	0.813
		0.15–0.20	438.488	24	0.177	0.204	0.619	0.796
		0.20–0.22	137.969	5	0.115	0.208	0.678	0.792
		0.22–0.23	438.318	20	0.146	0.219	0.635	0.781
		0.23–0.36	286.676	22	0.253	0.182	0.564	0.818
13	Circularity ratio	0.43–0.46	422.258	25	0.186	0.198	0.616	0.802
		0.46–0.50	557.112	30	0.169	0.209	0.622	0.791
		0.50–0.53	233.126	10	0.133	0.210	0.657	0.790
		0.53–0.59	206.166	17	0.266	0.184	0.549	0.816
		0.59–0.74	13.058	1	0.246	0.199	0.555	0.801

Table 6 (continued)

Sl. No	Parameter	Class	Area	No. of gully point	Belief	Disbelief	Uncertainty	Plausibility
14	Form factor	0.00–0.02	1061.907	65	0.177	0.170	0.653	0.830
		0.02–0.05	299.820	14	0.133	0.216	0.651	0.784
		0.05–0.11	10.857	1	0.276	0.204	0.521	0.796
		0.11–0.26	13.058	0	0.000	0.207	0.793	0.793
		0.26–1.40	46.079	3	0.189	0.204	0.607	0.796
15	Geology	Amphibolite and hornblende schist	235.248	10	0.001	0.104	0.895	0.896
		Clay with caliche	9.278	9	1.023	0.088	−0.111	0.912
		Granite	4.922	15	−0.047	0.080	0.967	0.920
		Granite gneiss and migmatite	661.786	30	0.002	0.118	0.880	0.882
		Intrusive granite	291.227	0	0.000	0.125	0.875	0.875
		Metamorphosed basic rocks	33.622	4	0.004	0.096	0.900	0.904
		Mica schist	197.296	14	0.002	0.095	0.903	0.905
		Quartz and pegmatite vein	3.197	1	0.014	0.097	0.888	0.903
		Quartzite and quartz schist	1.688	0	0.000	0.098	0.902	0.902
		River	4.109	0	0.000	0.099	0.901	0.901
16	Lineament density	0–0.036	469.706	27	0.206	0.201	0.593	0.799
		0.036–0.073	348.193	24	0.250	0.187	0.562	0.813
		0.073–0.110	288.245	16	0.199	0.203	0.599	0.797
		0.110–0.147	184.384	10	0.194	0.202	0.604	0.798
		0.147–0.184	140.737	6	0.151	0.206	0.643	0.794

possibilities (0.81–1.00) are found in the SW 1, 4, 5 and 15 which considered the role of optimistic beliefs. The high areas of potential for erosion (0.64–0.81) are concentrates found in SW 2, 3, 9, 12, 18, and 19 (Fig. 10a). The moderate potentiality of erosion (0.47–0.64) is found in SW 11, 13, 14, 16 and 17. The areas with low erosion potential are distributed in the SW 6, 7, and 8. The very low erosion potential (0.13–0.30) is only associated in SW 10. It was found that much of the watershed in this watershed is connected with moderate to very high potential for erosion which is the major risk to the vulnerability to erosion. The upper portion of this river basin is identified by high slope and rugged topography, and this zone is connected with numerous gully heads. This feature is strongly positive about the potentiality of erosion. Or else, the middle part of the river basin is connected with moderate to low vulnerability to erosion, but is extremely susceptible to erosion in the lower part due to human-induced disturbances and alteration of the reservoir relief element.

With the help of spatial logistic regression and its related breaking threshold in the GIS environment, the sub-basin-wise erosion possibilities were worked out. The very high potential for erosion (0.99–1.88) occurs in SW 2, 3, 4, 14 and 19. The high potential for erosion (0.47–0.99) is observed at t SW 12, 13, and 17. The moderate potentiality of erosion (0.40–0.47) is found in SW 1, 8, 9 and 16. The low erosion potential areas (0.18–0.40) are concentrated primarily in SW 5, 11, 15, and 18. The possibly very small erosion zones (0.01- 0.18) are located in SW 6, 7 and 10 (Fig. 10b). In this analysis, we find that high erosion potential reflects the upper and lower portion of the basin than the middle portion. The anthropogenic influence in the peak monsoon season results in a greater vulnerability to erosion due to the structural communications and the state of water logging.

With the aid of integrated EBF-SLR and their corresponding breaking thresholds in the GIS network, the sub-basin-wise erosion potentiality was calculated. The exceptionally high propensity for erosion (0.99–1.88) is observed in SW 1, 4, 5 and 12. The high effectiveness of erosion (0.47–0.99) is observed in SW 2, 3, 9, 13, 18 and 19. The moderate effectiveness of erosion (0.40–0.47) is found in SW 6, 11, 14, 16 and 17. The low erosion potential areas (0.18–0.40) are found primarily in the SW 7 and 8. The possibly very small erosion zones (0.01- 0.18) are located in SW 10 (Fig. 10c). In this method, we found that high erosion propensity characterizes the upper section of the region as compared to the middle and lower portion.

4.4 Accuracy assessment

The model's consistency depends on whether or not model matches reality of things then the theoretical model would be appropriate (Roy et al., 2020a). The ROC is the most accurate tool used for estimating the precision of the expected circumstance in different fields (Roy et al., 2020c). This method is used to determine the precision in different predicated models; frequency ratio, GWR, support vector machine, entropy model, advanced decision tree, analytical hierarchy process etc. Varying thresholds were regarded to determine the model's robustness for its sensitivity and specificity (Dou et al., 2019). Those analyzes are conducted as follows:

$$\text{Overall Accuracy} = \text{Number of Correct samples} \times \text{Total Samples}$$

$$K = \frac{\sum_{i=1}^{r} \text{Xii} - \sum_{i=1}^{r} (\text{xi}+ *_{xi} +i)}{N^2 - \sum_{i=1}^{r} (\text{xi}+ *_{xi} +i)} \quad (25)$$

The ROC AUC values were determined using the following equation to measure the exactness of the models predicted (Dou et al., 2019):

$$S_{\text{AUC}} = \sum_{k=1}^{n} (X_{k+1} - X_k) \left(S_k + 1 - S_{k+1} - \frac{S_k}{2} \right) \quad (26)$$

where S_{AUC} is the area under curve, X_k is the 1-Specificity and S_k is the compassion of the ROC (Chakrabortty et al., 2020c; Chen et al., 2021).

Thirty percent of all data was regarded for verification purposes in this study, the remainder of 70 percent of data used in the model of evidence-based belief function. For confirmation, a comprehensive field survey was conducted. From that study, we find that this research is correlated with a better degree of precision (Fig. 11). The AUC values of SLR, EBF and Ensemble EBF-SLR are 83.25, 90.01 and 92.54 simultaneously that represents greater precision and close to reality of things (Fig. 12). The Integrated EBF-SLR is much more practical than the EBF and SLR.
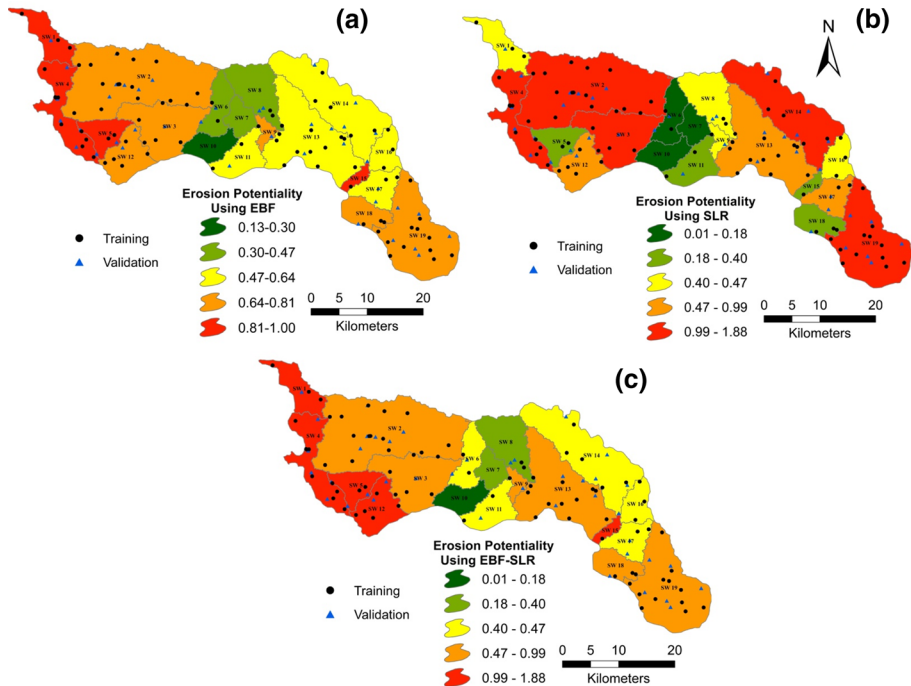
Fig. 10 Erosion Potentiality using: Evidential Belief Function (a), Spatial Logistic Regression (b), Ensemble Evidential Belief Function and Logistic Regression (c)

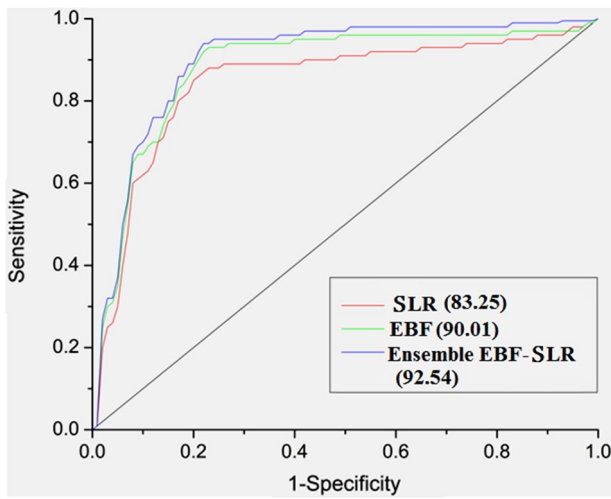**Fig. 11** Collection of field information regarding the amount of erosion

Fig. 12 Sensitivity Analysis

4.5 Soil erosion

The average annual soil erosion of this region is rangers between < 5.0 to > 35.0 tans/hac/year. Very high (> 35.0) soil erosion areas are found in the western, south-western, middle and some eastern portion of this region (Fig. 13). High (25.0–35.0) soil erosion areas are mainly found in the western and middle portion of this region. Moderate (15.0–25.0) soil erosion areas are mostly established in the western, middle and eastern portion of this region. Low (5.0–15.0) and very Low (5.0) soil erosion areas are primarily established in maximum part of this region. There is a positive relationship between erosion potentiality, occurrences of gullies and average annual soil erosion (Fig. 14). A major portion of this region is facing acute problem of land degradation owing to large-scale erosion like gullies. One of the major problems in the tropical and subtropical regions is extensive land loss due to gully erosion. The large amount of soil loss occurs in subtropical monsoon-dominated area due to several types of erosion such as board, rill and gullies. The unconsolidated materials are to a large degree removed from gullies formation. By reducing soil fertility, it directly impacts agricultural activity (Gayen et al., 2019; Zgłobicki et al., 2015). Thanks to the water-induced behavior, many environmental factors are ideal for the origin and growth of gullies. The gullies are usually categorized as permanent and ephemeral, in keeping with stability and occurrence (Foster, 1986). Permanent gullies are wide in existence and otherwise the ephemeral gullies are found during the wet season because of the large size of the runoff and its related water activity (Garosi et al., 2019). Favorable tillage activities change ephemeral gullies but the permanent gullies could not be altered by introducing this sort of interventions (Garosi et al., 2019; Roy et al., 2020b). The permanent as well as the ephemeral gullies are applied in this work to establish the training and validation
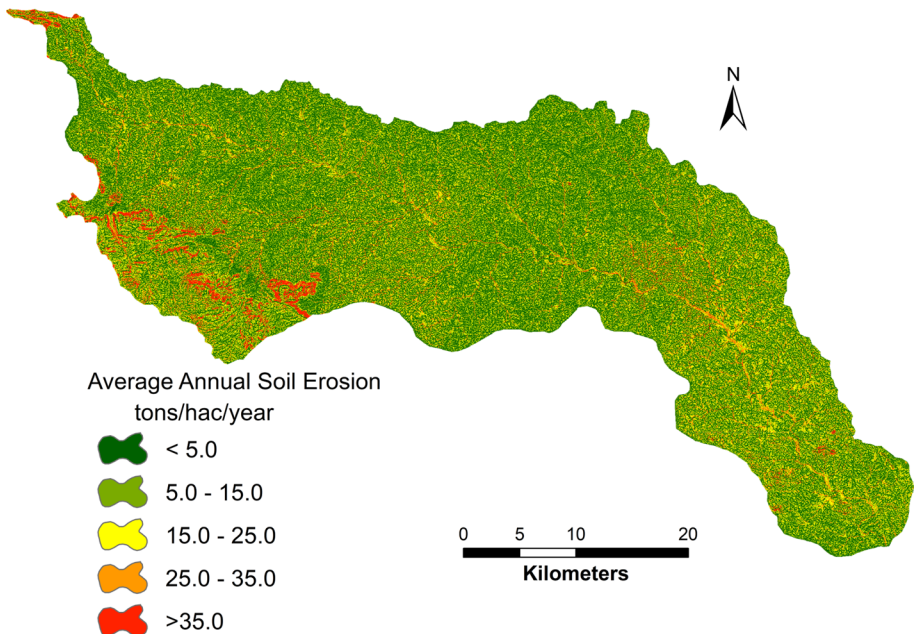

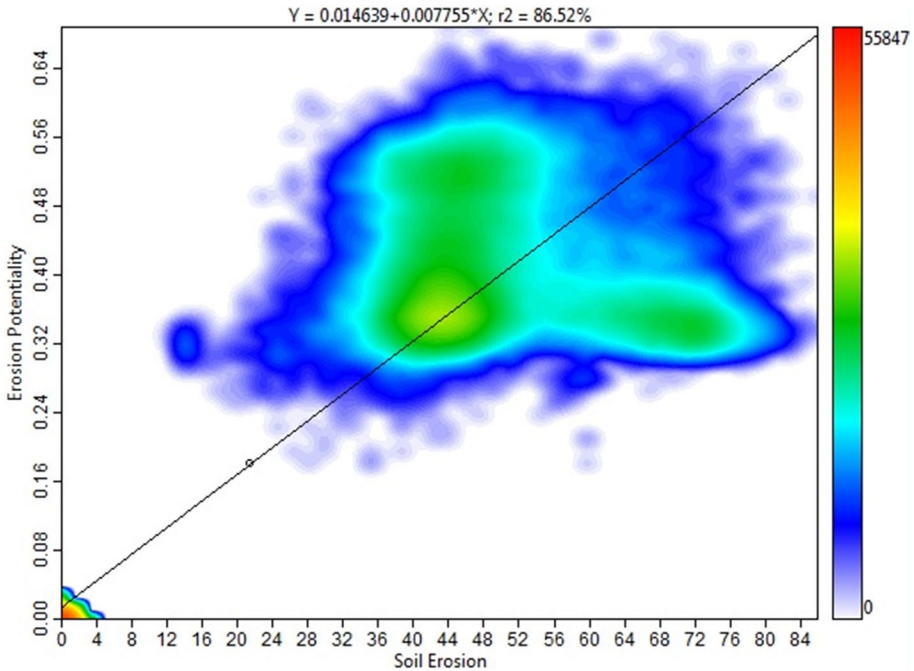**Fig. 13** Average annual soil erosion

Fig. 14 Relation between average annual soil erosion and erosion potentiality

datasets. In addition to the primary field knowledge, Google Earth and satellite imagery are regarded for creating the inventory map of the gully. The frequency of erosion is very strong in this area and there are so many gully points that are found during field visits. The handheld GPS is used to identify where gully head-cut is located. Favorable tillage activities change ephemeral gullies but the permanent gullies cannot be altered by introducing this sort of measures (Garosi et al., 2019). The large scale erosion in the form of formation and development of gullies apart from the declining fertility of soil, there is a negative impact on land and water resources (Li et al., 2016). Often the distinction among rills and gullies is very difficult without taking into account the cross-sectional area (Poesen, 1996). From the numerous research findings, it has been reported that the impact of gullies on soil loss as well as its related sedimentation is quite high (Sepuru & Dube, 2018).

5 Policy and managerial implications

As land degradation due to large-scale erosion is a vital issues in terms of the barriers of the environmental sustainability, the appropriate policy and its associated management are required from escaping this type of situation. Some soil and water conservation measures have been already implemented in this region for reducing the probability of erosion. With considering the nature and amount of erosion, different suggestive measures are shown:

  i.   The continuations of tillage farming have to be continuing in particularly in the time of Aush paddy cultivation. Aush is special type of rice which is cultivated in the month

of July–August in lower Gangetic plain of India. Traditional rice types and landraces according to the aus-type community (Oryza sativa L.) are considered to be highly resistant of ecological stresses variability such as drought and high temperature, and are thus valued genetic resources for sustainable agriculture.

ii. In the upper and middle part, the plantation program has to conduct with considering the local indigenous species, like Sal (Shorea robusta), Mahua (Madhuca longifolia), Palash (Butea monosperma) etc., the plantation of external species in the social forestry have to be limited for reducing the potentiality of erosion. The external species is capable to impact on the moisture content of soil in long term basis and modified the characteristics of soil.

iii. In the agricultural areas, particularly middle and lower portion of this region the traditional measures like field bunding have to be adopted in more optimal ways for reducing the initiation and development of rills and ephemeral gullies in the wet season. In very year, due to the formation of ephemeral gullies, a large scale of erosion has already been confirmed.

iv. Some structural and engineering measures have to be incorporated in the major erosion-prone region. In this perspective, the outcomes of erosion potentiality in sub-watershed scale should take a important part for taking the suitable remedies. In this perspective, the structural measures are suggested in SWS 1, 4, 5, 12 and 15 accordingly.

6 Conclusion

The implementation of integrated EBF-SLR method is quite dependable in estimating the possibilities for erosion as it interacts with the feature of belief from multiple sources, with disbelief, uncertainty and plausibility. Development of the probability-based database within the GIS platform not only consumes time and cost, but contracts with sufficient precision. The EBF-SLR ensemble is able of predicting the probability for erosion recognizing various factors of erosion causal factors and showing that the ROC AUC values are 92.54. Here, the AUC values from the ROC of SLR and EBF models are 83.25 and 90.01 respectively. Taking into account the EBF-SLR integrated, the SW like 1, 4, 5, 12, 15 are associated with very high erosion prospective areas and high erosion prospective zones are linked with SW like, 2, 3, 9, 13, 18, 19. There is a positive relationship, associated between erosion potentiality, existence of gullies and average annual soil erosion in this region. This region is experienced the water-induced large-scale erosion in monsoon period. Land degradation through large-scale erosion is one of the most effective concerns in this region. The declining productivity through land degradation is the main challenge of the agro-based society. From this analysis, it was revealed that most of the regions are connected with potentially very high to high erosion zones regarding the prospective for erosion. In this area, the correct solutions must be regarded for minimizing the quantity of erosion by integrating such structural and quasi-structural solutions with conservation into the local environmental perspective. Adapted land use and farming practices with appropriate plant distribution, water conservation methods will reduce the erosion level. Therefore, the structural measure may be implemented in the SW 2, 3, 6 and 10 to control the entire soil erosion-related factor to reduce the corrosion rates.

Based on the theoretical perspective of the gully erosion will be helpful to make conceptual awareness about the land degradation. The final result of this research work will be beneficial for the regional planners, stakeholders, and to the future researchers to take

suitable measurements for avoiding serious and immediate problem. It is because sometimes the flash flood destroys the weak upper surface soil with rapid flow and it can be controlled by following immediate protective for erosion. The western portion of this region is severally facing the acute problem of erosion by different forms of erosion. The rate of creation and development of gullies is maximum in this portion which accelerates the land degradation process rapidly. In erosion-prone region, some structural and non-structural measures can be taken into consideration. Field bunding, introduction of internal species with eradicating external species can be incorporated as a systemic measure. In some of the region of subtropical environment, the stakeholders already implemented the strategies regarding the measure for eradicating soil erosion, where subsistence-based agricultural practices already implemented from immemorial time. To link the sociopolitical and environmental dilemma, this contribution will help to develop the task of future research model with appropriate modification of the algorithm and partitioning of the samples.

References

Aher, P. D., Adinarayana, J., & Gorantiwar, S. D. (2014). Quantification of morphometric characterization and prioritization for management planning in semi-arid tropics of India: A remote sensing and GIS approach. *Journal of Hydrology*. https://doi.org/10.1016/j.jhydrol.2014.02.028

Alejandro, M., & Omasa, K. (2007). Estimation of vegetation parameter for modeling soil erosion using linear spectral mixture analysis of landsat ETM data. *ISPRS Journal of Photogrammetry and Remote Sensing, 62*, 309–324.

Arabameri, A., Asadi Nalivan, O., Saha, S., et al. (2020). Novel ensemble approaches of machine learning techniques in modeling the gully erosion susceptibility. *Remote Sensing, 12*, 1890. https://doi.org/10.3390/rs12111890

Arabameri, A., Chandra Pal, S., Costache, R., Saha, A., Rezaie, F., Seyed Danesh, A., & Hoang, N. D. (2021). Prediction of gully erosion susceptibility mapping using novel ensemble machine learning algorithms. *Geomatics, Natural Hazards and Risk, 12*(1), 469–498.

Avinash, K., Jayappa, K. S., & Deepika, B. (2011). Prioritization of sub-basins based on geomorphology and morphometricanalysis using remote sensing and geographic informationsystem (GIS) techniques. *Geocarto International*. https://doi.org/10.1080/10106049.2011.606925

Band, S. S., Janizadeh, S., Chandra Pal, S., et al. (2020a). Novel ensemble approach of deep learning neural network (DLNN) model and particle swarm optimization (PSO) algorithm for prediction of gully erosion susceptibility. *Sensors, 20*, 5609.

Band, S. S., Janizadeh, S., Chandra Pal, S., et al. (2020b). Flash flood susceptibility modeling using new approaches of hybrid and ensemble tree-based machine learning algorithms. *Remote Sensing, 12*, 3568.

Baskan, O. (2021). Analysis of spatial and temporal changes of RUSLE-K soil erodibility factor in semi-arid areas in two different periods by conditional simulation. *Archives of Agronomy and Soil Science*. https://doi.org/10.1080/03650340.2021.1922673

Bauwe, A., Kahle, P., & Lennartz, B. (2016). Hydrologic evaluation of the curve number and green and ampt infiltration methods by applying hooghoudt and kirkham tile drain equations using SWAT. *Journal of Hydrology, 537*, 311–321.

Bhave, A. G., Mishra, A., & Raghuwanshi, N. S. (2014). A combined bottom-up and top-down approach for assessment of climate change adaptation options. *Journal of Hydrology, 518*, 150–161. https://doi.org/10.1016/j.jhydrol.2013.08.039

Blaikie, P., & Brookfield, H. (2015). *Land degradation and society*. Routledge.

Cetin, M. (2015a). Consideration of permeable pavement in landscape architecture. *Journal of Environmental Protection and Ecology, 16*, 385–392.

Cetin, M. (2015b). Using GIS analysis to assess urban green space in terms of accessibility: Case study in Kutahya. *International Journal of Sustainable Development & World Ecology, 22*, 420–424.

Cetin, M. (2015c). Determining the bioclimatic comfort in Kastamonu City. *Environmental Monitoring and Assessment, 187*, 640.

Cetin, M., & Sevik, H. (2016a). Evaluating the recreation potential of Ilgaz mountain national park in Turkey. *Environmental Monitoring and Assessment, 188*, 52.

Cetin M, Sevik H (2016b) Assessing potential areas of ecotourism through a case study in Ilgaz Mountain National Park. Tourism-from empirical research towards practical application 81–110

Cetin, M., Sevik, H., Canturk, U., & Cakir, C. (2018a). Evaluation of the recreational potential of Kutahya Urban Forest. *Fresenius Environmental Bulletin, 27*, 2629–2634.

Cetin, M., Zeren, I., Sevik, H., et al. (2018b). A study on the determination of the natural park's sustainable tourism potential. *Environmental Monitoring and Assessment, 190*, 167.

Cetin, M., Adiguzel, F., Gungor, S., et al. (2019). Evaluation of thermal climatic region areas in terms of building density in urban management and planning for Burdur, Turkey. *Air Quality, Atmosphere & Health, 12*, 1103–1112.

Chakrabortty, R., Pal, S. C., Chowdhuri, I., et al. (2020a). Assessing the importance of static and dynamic causative factors on erosion potentiality using SWAT, EBF with uncertainty and plausibility, logistic regression and novel ensemble model in a sub-tropical environment. *Journal of the Indian Society of Remote Sensing, 48*, 765–789. https://doi.org/10.1007/s12524-020-01110-x

Chakrabortty, R., Pal, S. C., Sahana, M., et al. (2020b). Soil erosion potential hotspot zone identification using machine learning and statistical approaches in eastern India. *Natural Hazards, 104*, 1259–1294. https://doi.org/10.1007/s11069-020-04213-3

Chakrabortty, R., Pradhan, B., Mondal, P., & Pal, S. C. (2020c). The use of RUSLE and GCMs to predict potential soil erosion associated with climate change in a monsoon-dominated region of eastern India. *Arabian Journal of Geosciences, 13*, 1–20.

Chen, J. (2007). Rapid urbanization in China: A real challenge to soil protection and food security. *CATENA, 69*, 1–15.

Chen, W., Lei, X., Chakrabortty, R., et al. (2021). Evaluation of different boosting ensemble machine learning models and novel deep learning and boosting framework for head-cut gully erosion susceptibility. *Journal of Environmental Management, 284*, 112015.

Chowdary, V. M., Ramakrishnan, D., Srivastava, Y. K., et al. (2009). Integrated water resource development plan for sustainable management of mayurakshi watershed India using remote sensing and GIS. *Water Resources Management*. https://doi.org/10.1007/s11269-008-9342-9

Chowdhuri, I., Pal, S. C., Arabameri, A., et al. (2020). Implementation of artificial intelligence based ensemble models for gully erosion susceptibility assessment. *Remote Sensing, 12*, 3620. https://doi.org/10.3390/rs12213620

Clarke, J. (1966). *Morphometry from maps*. Heinmann, London: Essays in geomorphology.

Dempster, A. P. (1968). Upper and lower probabilities generated by a random closed interval. *The Annals of Mathematical Statistics, 39*, 957–966.

Dou, J., Yunus, A. P., Tien Bui, D., et al. (2019). Assessment of advanced random forest and decision tree algorithms for modeling rainfall-induced landslide susceptibility in the Izu-Oshima Volcanic Island Japan. *Science of the Total Environment*. https://doi.org/10.1016/j.scitotenv.2019.01.221

Enters, T. (1998). *Methods for the economic assessment of the on-and off-site impacts of soil erosion*. IBSRAM Bangkok.

Erener, A., & Düzgün, H. (2012). Landslide susceptibility assessment: What are the effects of mapping unit and mapping method? *Environmental Earth Sciences, 66*, 859–877.

Fadil, A., Rhinane, H., Kaoukaya, A., et al. (2011). Hydrologic modeling of the bouregreg watershed (Morocco) using GIS and SWAT model. *Journal of Geographic Information System*. https://doi.org/10.4236/jgis.2011.34024

Feizizadeh, B., Blaschke, T., & Nazmfar, H. (2014). GIS-based ordered weighted averaging and Dempster-Shafer methods for landslide susceptibility mapping in the Urmia Lake Basin Iran. *International Journal of Digital Earth, 7*, 688–708.

Foster, G. (1986). Understanding Ephemeral Gully Erosion. *Soil Conservation, 2*, 90–125.

Full article: Prediction of gully erosion susceptibility mapping using novel ensemble machine learning algorithms. Accessed 27 May 2021 https://www.tandfonline.com/doi/full/https://doi.org/10.1080/19475705.2021.1880977

Gajbhiye, S., Mishra, S. K., & Pandey, A. (2014). Prioritizing erosion-prone area through morphometric analysis: An RS and GIS perspective. *Applied Water Science*. https://doi.org/10.1007/s13201-013-0129-7

Garosi, Y., Sheklabadi, M., Conoscenti, C., et al. (2019). Assessing the performance of GIS-based machine learning models with different accuracy measures for determining susceptibility to gully erosion. *Science of the Total Environment, 664*, 1117–1132.

Gayen, A., Pourghasemi, H. R., Saha, S., et al. (2019). Gully erosion susceptibility assessment and management of hazard-prone areas in India using different machine learning algorithms. *Science of the Total Environment, 668*, 124–138.

Gelagay, H. S., & Minale, A. S. (2016). Soil loss estimation using GIS and Remote sensing techniques: A case of Koga watershed Northwestern Ethiopia. *International Soil and Water Conservation Research*. https://doi.org/10.1016/j.iswcr.2016.01.002

Ghosh, S., & Guchhait, S. K. (2016). Geomorphic threshold estimation for gully erosion in the lateritic soil of birbhum West Bengal India. SOIL Discussions. https://doi.org/10.5194/soil-2016-48

Gorsevski, P. V., Gessler, P. E., Foltz, R. B., & Elliot, W. J. (2006). Spatial prediction of landslide hazard using logistic regression and ROC analysis. *Transactions in GIS, 10*, 395–415.

Hembram, T. K., & Saha, S. (2020). Prioritization of sub-watersheds for soil erosion based on morphometric attributes using fuzzy AHP and compound factor in Jainti river basin, Jharkhand, Eastern India. *Environment, Development and Sustainability, 22*, 1241–1268. https://doi.org/10.1007/s10668-018-0247-3

Horton, R. E. (1932). Drainage-Basin Characteristics. *Transactions AGU, 13*, 350. https://doi.org/10.1029/TR013i001p00350

Horton, R. E. (1945). Erosional development of streams and their drainage basins; hydrophysical approach to quantitative morphology. *Geol Soc America Bull, 56*, 275. https://doi.org/10.1130/0016-7606(1945)56[275:EDOSAT]2.0.CO;2

Kanth, T., & Hassan, Z. (2012). Morphometric analysis and prioritization of watersheds for soil and water resource management in Wular catchment using geo-spatial tools. *International Journal of Geology, Earth and Environmental Sciences, 2*, 30–41.

Kaya, E., Agca, M., Adiguzel, F., & Cetin, M. (2019). Spatial data analysis with R programming for environment. *Human and Ecological Risk Assessment: An International Journal, 25*, 1521–1530.

Kelson, K. I., & Wells, S. G. (1989). Geologic influences on fluvial hydrology and bedload transport in small mountainous watersheds Northern New Mexico USA. *Earth Surface Processes and Landforms*. https://doi.org/10.1002/esp.3290140803

Korb, K. B., & Nicholson, A. E. (2010). *Bayesian artificial intelligence*. CRC Press.

Koskivaara, E. (2004). *Artificial neural networks in analytical review procedures*. Managerial Auditing Journal.

Kottagoda, S., & Abeysingha, N. (2017). Morphometric analysis of watersheds in Kelani river basin for soil and water conservation. *Journal of the National Science Foundation of Sri Lanka, 45*, 6.

Kouli, M., Soupios, P., & Vallianatos, F. (2009). Soil erosion prediction using the revised universal soil loss equation (RUSLE) in a GIS framework Chania Northwestern Crete Greece. *Environmental Geology*. https://doi.org/10.1007/s00254-008-1318-9

Lal, R. (2003). Soil erosion and the global carbon budget. *Environment International, 29*(4), 437–450.

Lal, R. (2014). Soil conservation and ecosystem services. *International Soil and Water Conservation Research*. https://doi.org/10.1016/S2095-6339(15)30021-6

Lee, S. (2007). Comparison of landslide susceptibility maps generated through multiple logistic regression for three test areas in Korea. *Earth Surface Processes and Landforms: THe Journal of the British Geomorphological Research Group, 32*, 2133–2148.

Li, Y., Jiao, J., Wang, Z., et al. (2016). Effects of revegetation on soil organic carbon storage and erosion-induced carbon loss under extreme rainstorms in the hill and gully region of the loess plateau. *IJERPH, 13*, 456. https://doi.org/10.3390/ijerph13050456

Lin, C. Y., Lin, W. T., & Chou, W. C. (2002). Soil erosion prediction and sediment yield estimation: The Taiwan experience. *Soil and Tillage Research*. https://doi.org/10.1016/S0167-1987(02)00114-9

Liu, X., Jia, G., Yu, X. (2021). Effects of the undecomposed layer and semi-decomposed layer of Quercus variabilis litter on the soil erosion process and the eroded sediment particle size distribution. *Hydrological Processes*. https://doi.org/10.1002/hyp.14195

Malik, S., Pal, S. C., Das, B., & Chakrabortty, R. (2019). *Assessment of vegetation status of Sali River basin a tributary of Damodar river in Bankura West Bengal using satellite data* (pp. 1–35). Development and Sustainability: Environment.

Malpica, J. A., Alonso, M. C., & Sanz, M. A. (2007). Dempster-Shafer Theory in geographic information systems: A survey. *Expert Systems with Applications, 32*, 47–55.

Martınez, A., Dimitriadis, Y., Rubia, B., et al. (2003). Combining qualitative evaluation and social network analysis for the study of classroom social interactions. *Computers & Education, 41*, 353–368.

Meshram, S. G., & Sharma, S. K. (2017). Prioritization of watershed through morphometric parameters: A PCA-based approach. *Applied Water Science*. https://doi.org/10.1007/s13201-015-0332-9

Miller VC (1953). Quantitative geomorphic study of drainage basin characteristics in the Clinch Mountain area, Virginia and Tennessee. Technical report (Columbia University Department of Geology); no 3

Mittal, N., Mishra, A., Singh, R., et al. (2014). Flow regime alteration due to anthropogenic and climatic changes in the Kangsabati River, India. *Ecohydrology & Hydrobiology, 14*, 182–191.

Moglen, G. E., Eltahir, E. A. B., & Bras, R. L. (1998). On the sensitivity of drainage density to climate change. *Water Resources Research*. https://doi.org/10.1029/97WR02709

Mohammadi, S., Balouei, F., Haji, K., et al. (2021). Country-scale spatio-temporal monitoring of soil erosion in Iran using the G2 model. *International Journal of Digital Earth*. https://doi.org/10.1080/17538947.2021.1919230

Mostaghimi, S., Brannan, K. M., Dillaha III, T. A., & Bruggeman, A. C. (2000). Best management practices for nonpoint source pollution control: Selection and assessment. In *Agricultural Nonpoint Source Pollution; Water Management and Hydrology,* (Ch. 10, pp. 91–109).

Nasir Ahmad, N. S. B., Mustafa, F. B., Yusoff, M., S, Y, & Didams, G. (2020). A systematic review of soil erosion control practices on the agricultural land in Asia. *International Soil and Water Conservation Research, 8*, 103–115. https://doi.org/10.1016/j.iswcr.2020.04.001

Nearing MA (2013). Soil Erosion and Conservation. In: Environmental Modelling: Finding Simplicity in Complexity: Second Edition

Oguchi, T. (1997). Drainage density and relative relief in humid steep mountains with frequent slope failure. *Earth Surface Processes and Landforms*. https://doi.org/10.1002/(SICI)1096-9837(199702)22:2%3c107::AID-ESP680%3e3.0.CO;2-U

Oldeman LR (1992) Global extent of soil degradation. In: Bi-Annual Report 1991–1992/ISRIC. ISRIC, pp 19–36

Oliver, M. A., & Gregory, P. (2015). Soil, food security and human health: A review. *European Journal of Soil Science, 66*, 257–276.

Ozdemir, H., & Bird, D. (2009). Evaluation of morphometric parameters of drainage networks derived from topographic maps and DEM in point of floods. *Environmental Geology, 56*, 1405–1415.

Pal, S. C., & Chakrabortty, R. (2019a). Simulating the impact of climate change on soil erosion in subtropical monsoon dominated watershed based on RUSLE, SCS runoff and MIROC5 climatic model. *Advances in Space Research, 64*, 352–377.

Pal, S. C., & Chakrabortty, R. (2019b). Modeling of water induced surface soil erosion and the potential risk zone prediction in a sub-tropical watershed of Eastern India. *Modeling Earth Systems and Environment, 5*, 369–393.

Pal, S. C., & Shit, M. (2017). Application of RUSLE model for soil loss estimation of Jaipanda watershed, West Bengal. *Spatial Information Research, 25*, 399–409.

Pal, S. C., Chakrabortty, R., Malik, S., & Das, B. (2018). Application of forest canopy density model for forest cover mapping using LISS-IV satellite data: A case study of Sali watershed, West Bengal. *Model Earth Syst Environ, 4*, 853–865. https://doi.org/10.1007/s40808-018-0445-x

Pal, S. C., Arabameri, A., Blaschke, T., et al. (2020). Ensemble of machine-learning methods for predicting gully erosion susceptibility. *Remote Sensing, 12*, 3675. https://doi.org/10.3390/rs12223675

Pal, S. C., Chakrabortty, R., Roy, P., et al. (2021). Changing climate and land use of 21st century influences soil erosion in India. *Gondwana Research, 94*, 164–185. https://doi.org/10.1016/j.gr.2021.02.021

Pareta, K., & Pareta, U. (2011). Quantitative Morphometric Analysis of a Watershed of Yamuna Basin, India using ASTER DEM Data and GIS. *International Journal of Geomatics and Geosciences., 2*(1), 248.

Patel, D. P., Gajjar, C. A., & Srivastava, P. K. (2013). Prioritization of Malesari mini-watersheds through morphometric analysis: A remote sensing and GIS perspective. *Environment and Earth Science, 69*, 2643–2656. https://doi.org/10.1007/s12665-012-2086-0

Pimentel, D. (2006). Soil erosion: A food and environmental Threat. *Environment, Development and Sustainability, 8*, 119–137. https://doi.org/10.1007/s10668-005-1262-8

Poesen J (1996) Contribution of gully erosion to sediment production. IAHS, p 251

Pradhan, B. (2010). Landslide susceptibility mapping of a catchment area using frequency ratio, fuzzy logic and multivariate logistic regression approaches. *Journal of the Indian Society of Remote Sensing, 38*, 301–320.

Rahmati, O., Haghizadeh, A., & Stefanidis, S. (2016). Assessing the accuracy of GIS-based analytical hierarchy process for watershed prioritization Gorganrood river basin Iran. *Water Resources Management*. https://doi.org/10.1007/s11269-015-1215-4

Rai, P. K., Chandel, R. S., Mishra, V. N., & Singh, P. (2018). Hydrological inferences through morphometric analysis of lower Kosi river basin of India for water resource management based on remote sensing data. *Applied Water Science, 8*, 15.

Renard KG, Yoder DC, Lightle DT, Dabney SM (2011). Universal Soil Loss Equation and Revised Universal Soil Loss Equation. In: Handbook of Erosion Modelling

Richard SM (1968) Unclassified ad number

Roy, P., Chakrabortty, R., Chowdhuri, I., et al. (2020a). Development of Different Machine Learning Ensemble Classifier for Gully Erosion Susceptibility in Gandheswari Watershed of West Bengal,

India. In J. K. Rout, M. Rout, & H. Das (Eds.), *Machine Learning for Intelligent Decision Science.* Singapore: Springer Singapore.

Roy, P., Chandra Pal, S., Arabameri, A., et al. (2020b). Novel ensemble of multivariate adaptive regression spline with spatial logistic regression and boosted regression tree for gully erosion susceptibility. *Remote Sensing, 12*, 3284.

Roy, P., Chandra Pal, S., Chakrabortty, R., et al. (2020c). Threats of climate and land use change on future flood susceptibility. *Journal of Cleaner Production, 272*, 122757. https://doi.org/10.1016/j.jclepro.2020.122757

Saha, A., Ghosh, M., & Pal, S. C. (2020). Understanding the Morphology and Development of a Rill-Gully: An Empirical Study of Khoai Badland, West Bengal, India. In P. K. Shit, H. R. Pourghasemi, & G. S. Bhunia (Eds.), *Gully Erosion Studies from India and Surrounding Regions* (pp. 147–161). Springer International Publishing.

Saha, A., Pal, S. C., Arabameri, A., et al. (2021). Optimization modelling to establish false measures implemented with ex-situ plant species to control gully erosion in a monsoon-dominated region with novel in-situ measurements. *Journal of Environmental Management, 287*, 112284. https://doi.org/10.1016/j.jenvman.2021.112284

Sahour, H., Gholami, V., Vazifedan, M., & Saeedi, S. (2021). Machine learning applications for water-induced soil erosion modeling and mapping. *Soil and Tillage Research, 211*, 105032. https://doi.org/10.1016/j.still.2021.105032

Schumm, S. A. (1956). *Evolution of drainage systems and slopes in badlands at Perth Amboy.* Bulletin of the Geological Society of America. https://doi.org/10.1130/0016-7606(1956)67[597:EODSAS]2.0.CO;2

Sepuru, T. K., & Dube, T. (2018). An appraisal on the progress of remote sensing applications in soil erosion mapping and monitoring. *Remote Sensing Applications: Society and Environment, 9*, 1–9. https://doi.org/10.1016/j.rsase.2017.10.005

Sreedevi, P., Owais, S., Khan, H., & Ahmed, S. (2009). Morphometric analysis of a watershed of South India using SRTM data and GIS. *Journal of the Geological Society of India, 73*, 543–552.

Strahler, A. N. (1957). Quantitative analysis of watershed geomorphology. *Eos, Transactions American Geophysical Union.* https://doi.org/10.1029/TR038i006p00913

Strahler, A. N. (1964). *Part II Quantitative geomorphology of drainage basins and channel networks* (pp. 4–39). Handbook of Applied Hydrology: McGraw-Hill, New York.

Tehrany, M. S., Shabani, F., Javier, D. N., & Kumar, L. (2017). Soil erosion susceptibility mapping for current and 2100 climate conditions using evidential belief function and frequency ratio. *Geomatics, Natural Hazards and Risk, 8*, 1695–1714.

Teng, H., Liang, Z., Chen, S., et al. (2018). Current and future assessments of soil erosion by water on the Tibetan Plateau based on RUSLE and CMIP5 climate models. *Science of the Total Environment.* https://doi.org/10.1016/j.scitotenv.2018.04.146

Thomas, A., Snyder, W., Mills, W., & Dillard, A. (1991). Erosion risk assessment for soil conservation planning. *Soil Technology, 4*, 373–389.

Tian, P., Zhu, Z., Yue, Q., et al. (2021). Soil erosion assessment by RUSLE with improved P factor and its validation: Case study on mountainous and hilly areas of Hubei Province China. *International Soil and Water Conservation Research.* https://doi.org/10.1016/j.iswcr.2021.04.007

B. Wg V., Thornbury WD. (2006). Principles of geomorphology. *The Geographical Journal.* https://doi.org/10.2307/1791828

Wischmeier WH, Smith DD (1978). Predicting Rainfall Erosion Losses : a guide to conservation planning. Agriculture Handbook

Yadav, S. K., Singh, S. K., Gupta, M., & Srivastava, P. K. (2014). Morphometric analysis of upper tons basin from Northern Foreland of peninsular India using CARTOSAT satellite and GIS. *Geocarto International.* https://doi.org/10.1080/10106049.2013.868043

Yang, J., Song, C., Yang, Y., et al. (2019). New method for landslide susceptibility mapping supported by spatial logistic regression and GeoDetector: A case study of Duwen Highway Basin, Sichuan Province, China. *Geomorphology, 324*, 62–71.

Yilmaz, I. (2009). Landslide susceptibility mapping using frequency ratio, logistic regression, artificial neural networks and their comparison: A case study from Kat landslides (Tokat—Turkey). *Computers & Geosciences, 35*, 1125–1138.

Zgłobicki, W., Baran-Zgłobicka, B., Gawrysiak, L., & Telecka, M. (2015). The impact of permanent gullies on present-day land use and agriculture in loess areas (E. Poland). *CATENA, 126*, 28–36. https://doi.org/10.1016/j.catena.2014.10.022

Authors and Affiliations

Rabin Chakrabortty[1] · Subodh Chandra Pal[1] [ID] · Alireza Arabameri[2] · Phuong Thao Thi Ngo[3] · Indrajit Chowdhuri[1] · Paramita Roy[1] · Sadhan Malik[1] · Biswajit Das[1]

Rabin Chakrabortty
rabingeo8@gmail.com

Alireza Arabameri
alireza.ameri91@yahoo.com

Phuong Thao Thi Ngo
Ngotphuongthao5@duytan.edu.vn

Indrajit Chowdhuri
indrajitchowdhuri@gmail.com

Paramita Roy
paramitaroy95@gmail.com

Sadhan Malik
sadhanmalik06@gmail.com

Biswajit Das
biswajitdas1119@gmail.com

[1]   Department of Geography, The University of Burdwan, Bardhaman 713104, West Bengal, India

[2]   Department of Geomorphology, Tarbiat Modares University, Tehran 14117-13116, Iran

[3]   Institute of Research and Development, Duy Tan University, Da Nang 550000, Vietnam